Biomaterials Science

ROYAL SOCIETY OF CHEMISTRY

REVIEW

View Article Online
View Journal | View Issue

Cite this: *Biomater. Sci.*, 2023, **11**, 5727

Microneedle-based glucose monitoring: a review from sampling methods to wearable biosensors

Yan Wang,[a] You Wu[a] and Yifeng Lei *[a,b]

Received 8th March 2023,
Accepted 25th June 2023

DOI: 10.1039/d3bm00409k

rsc.li/biomaterials-science

Blood glucose (BG) monitoring is critical for diabetes management. In recent years, microneedle (MN)-based technology has attracted emerging attention in glucose sensing and detection. In this review, we summarized MN-based sampling for glucose collection and glucose analysis in detail. First, different principles of MN-based biofluid extraction were elaborated, including external negative pressure, capillary force, swelling force and iontophoresis, which would guide the shape design and material optimization of MNs. Second, MNs coupled with different analysis approaches, including Raman methods, colorimetry, fluorescence, and electrochemical sensing, were emphasized to exhibit the trend towards highly integrated wearable sensors. Finally, the future development prospects of MN-based devices were discussed.

1. Introduction

Diabetes mellitus (DM) is a group of metabolic diseases characterized by a failure of regulation of blood glucose (BG) levels in the body, and has become a challenging health problem worldwide.[1] According to the latest statistics from the International Diabetes Federation (IDF) in 2021, 537 million people worldwide live with DM, and China tops the chart with the highest number of diabetic patients (140.9 million).[1] Not only does DM create secondary health complications, if uncontrolled, it can also lead to high chronic mortality rates.[2,3] The prevalence of this epidemic morbidity is ever-increasing and seriously threatens global socio-economic welfare.

Intensive diabetes treatment reduces the risk of complications, and glucose monitoring is a core component of successful management in diabetes.[1] Blood tests have long been the gold standard for clinical diagnosis. The common method of glucose monitoring involves sampling a small amount of blood from a patient's fingerstick. However, frequent blood sampling can create pain and is inconvenient, with the potential risk for cross-contamination, which creates trypanophobia in many diabetic patients. To avoid traditional BG monitoring, numerous alternative techniques have been developed, from invasive towards minimally invasive and non-invasive glucose monitoring, which mainly includes non-invasive optical methods,[4–6] sampling from other sites instead of the fingertip, and wireless continuous glucose monitoring (CGM).[7–10]

Sweat,[8,11,12] saliva,[13] tears,[14,15] and interstitial fluid (ISF) are common alternative test samples for BG monitoring. In comparison with the other peripheral biofluids, ISF contains

[a]*School of Power and Mechanical Engineering & The Institute of Technological Science, Wuhan University, Wuhan 430072, China. E-mail: yifenglei@whu.edu.cn*
[b]*Wuhan University Shenzhen Research Institute, Shenzhen 518057, China*

Yan Wang

Miss Yan Wang is currently a master's student at the School of Power and Mechanical Engineering, Wuhan University. She received her B.S. degree in Biomedical Engineering from Southwest Jiaotong University in 2021. Her research interests include medical materials, the preparation and application of microneedles, as well as photonic crystal hydrogel sensors.

You Wu

Miss You Wu is a master's student at the School of Power and Mechanical Engineering, Wuhan University. She received her B.S. degree in Materials Science and Engineering from Wuhan University in 2021. Her research interests focus on the design and application of microneedles, MEMS sensors and actuators, and microfluidic devices.

abundant physiological information and exhibits a close correlation with blood samples due to the transcapillary exchange between the blood and the cells.[16] ISF is contained in all layers of the skin below the stratum corneum, accounting for 45% of the skin volume (blood accounts for only 5%), with non-clotting properties and high sensitivity to local tissue changes.[17] Thus, ISF has gained popularity as a biomarker source to diagnose DM, owing to its ability to provide glucose trends and fluctuations.[18] However, relevant detection methods are limited by the low permeability of the human skin to glucose due to the outermost stratum corneum layer. A variety of approaches have been suggested to enhance the extraction of ISF (*i.e.* suction blisters, sonication, electric fields, or reverse iontophoresis[19–22]); however, these methods would alter the composition of the ISF, due to the local trauma caused by the extraction process. Although a transdermal ISF extraction technique using ultrasound and vacuum offers the promise of non-invasive, continuous, and real-time glucose monitoring, this technique only extracts a minimal volume of ISF, which scatters on the skin surface, making it unsuitable for ISF collection and measurement by using macroscale systems.

In recent years, microneedles (MNs) have gained significant attention due to their micron size and minimal invasion.[23,24] MNs are been extensively exploited in biofluid extraction,[25] bacterial sensing,[26] transdermal detection,[27,28] as well as transdermal drug delivery for various diseases including diabetes.[29,30] In particular, MNs are widely used in ISF sampling and measuring unique biomarkers for disease diagnosis, prognosis, and treatment because of the painless experience and desired patient compliance. Zhang *et al.* developed encoded MNs capable of detecting multiple biomarkers in skin ISF.[31] Yang *et al.* reported an MN array encapsulated with programmed DNA hydrogels for the sensitive detection of miRNA in ISF.[32] Wang *et al.* designed an MN patch for fast *in vivo* sampling and on-needle ultrasensitive quantification of target protein biomarkers in ISF.[33]

At present, ISF direct extraction and electrochemical probes are two types of MN-based technology applied in medical sensing. In this review, we focus on the development and application of MN-based sampling, detection and sensing devices. First, we introduce the extraction principles to guide the shape design and material optimization of MNs (Fig. 1, top and middle panels). Second, we present the current performance and potential scenarios of different types of MN-based transdermal diagnosis approach, including Raman method, colorimetry, and fluorescence (Fig. 1, bottom panel). Later, the integration of MNs as probes or biofluid collectors with electrochemical sensors (Fig. 1, bottom panel) for continuous glucose detection is highlighted to elaborate the trend towards highly integrated sensors. Finally, the current challenges and the perspectives on future development are also discussed to fulfill the great potential of MN technology.

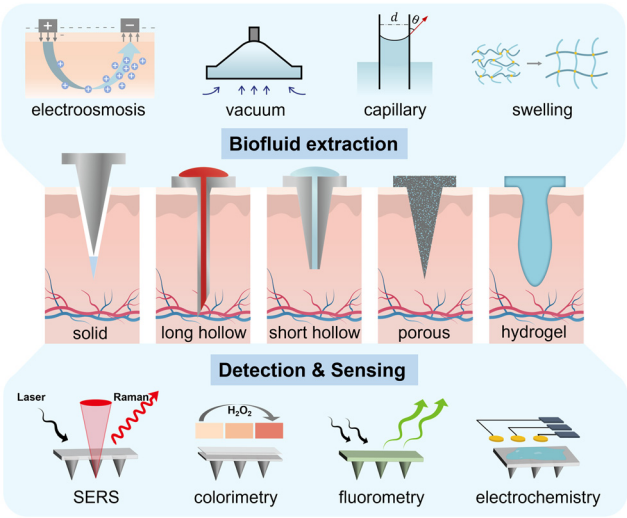

Fig. 1 Schematic illustration of different shapes of MNs, MN-mediated biofluid extraction and diagnosis system for glucose monitoring.

2. MNs for biofluid extraction

MNs, as a sampling tool, construct a bridge between the biofluids and the reservoir, allowing ISF and blood to be extracted with the assistance of negative pressure, capillary force, swelling force, or electroosmosis.[34] Four types of MN (solid MNs, hollow MNs, porous MNs, and swelling MNs) have been extensively used for transdermal sampling (Fig. 1, middle panel). The collected biofluids can be transported out of the device for analysis using established analytical methods. In the following we will introduce different principles of MN-based ISF extraction, and illustrate the relevant shape design and material optimization of MN systems (Table 1).

2.1. Negative pressure-based extraction

Negative pressure-based extraction drives the biofluid flow through pressure differences between the skin and the MNs (Fig. 1).[35] The extraction is initiated with a vacuum actuator, which is pre-stored or press-generated, and is usually com-

Yifeng Lei

Dr Yifeng Lei is an Assistant Professor at the School of Power and Mechanical Engineering, Wuhan University. Dr Lei obtained her Ph.D. degree from the University of Bordeaux, France, in 2013. She carried out post-doc research at the National Center for Nanoscience and Nanotechnology, China, before joining Wuhan University in 2016. Dr Lei's group's research interests include biomaterials, 3D bioprinting, flexible electronics, and wearable medical devices.

Table 1 Comparison of MN-based biofluid extraction

Extraction principle	Targets	MN specifications	MN body materials	MN fabrication method	Related equipment	Sampling volume/rate	Sampling time	Test subject	Ref.
Negative pressure	Glucose and cholesterol in blood	Single HMN, 1800 μm length	Metal/ parylene	Drawing lithography	Paper-based sensor with a PDMS switch	30 ± 5 μL blood	10 s	Rabbit	37
	Blood	30 SMNs, 1000 μm length	SS	N.R.	An insertion mechanism, stored vacuum, and a microfluidic system containing lithium heparin anticoagulant	100 μL of anticoagulant-mixed blood	3 min	Human	25
	ISF	Single HMN, 1500 μm length	SS	N.R.	The open concentric design at the MN base	2 μL ISF	10–15 min	Rat and human	16
	Glucose in ISF	HMNs, 700–1500 μm length	Glass	Thermal puller	A vacuum of −66.5 to −26.6 kPa	1–10 μL ISF	2–10 min	Rat and human	35
	ISF	5 SMNs, 250–650 μm length	SS	Photoetching	A vacuum of −50 kPa	2.3 ± 2.6 μL ISF	20 min	Human	17
	Glucose in ISF	10 × 10 array of HMNs, 900 μm length	Maltose/ MeHA	Micromolding	An electronic glucose sensor	3.82 μL ISF	3 min	Pig skin, rat	40
Capillary action	Glucose in ISF	20 × 20 array of HMNs, 250–350 μm length	Silicon	Etching oxidation, photolithographic patterning and DRIE	A commercial blood glucose test strip	N.R.	15–20 min	Human	42
	Glucose in ISF	1×10^6 needles per cm^2 HMN, 100 μm length	Silicon	Lithography, BHF etching	Enzymatic glucose biosensor	1 μL s^{-1}	N.R.	Glucose solutions	43
	ISF	HMNs, 150 μm length	Silicon	DRIE	N.R.	N.R.	N.R.	Pig skin	44
	Glucose in ISF	Single HMN, 700 μm length	Silicon	Isotropic, anisotropic dry etching	An electrochemical sensing probe in the lumen of a single HMN	N.R.	10 min	Human	45
	Glucose in ISF	5 × 5 array of PMNs, 900 μm length	Alumina/ epoxy resin	Centrifugal casting, sintering	The Amplex red glucose/glucose oxidase kit	N.R.	15 min	Agarose gel	47
	ISF	6 × 6 array of PMNs, 700 μm length	PGMA	Sacrificial pore-causing agents	N.R.	N.R.	N.R.	Pig skin, agarose gel	50
	Glucose and cholesterol in ISF	12 × 12 array of PMNs, 680 μm length	PVF	Micromolding	A glucose assay kit, cholesterol quantitation kit	3.6 ± 0.6 mg ISF	5 min	Rat	51
	Endotoxin in ISF	10 × 10 array of PMNs, 950 μm length	ETPTA	Sacrificial pore-causing agents	Microplate reader	LOD: 0.0064 EU ml^{-1}	1 h	Rat	52
	Glucose in ISF	21 PMNs, 900 μm length	HA/PDMS	Salt leaching method	A microfluidic system, a glucose test paper	0.667 μL min^{-1}	N.R.	Agarose gel	53
	Cystatin C in blood	10 PMNs, 1800 μm length	PLGA/ maltose	Thermal puller, EtOH–NaOH treatment	A plasmonic paper and a homemade benchtop absorbance setup	50 μL blood	2 min	Human	54
	ISF	PEG-coated PSF MNs	PDA/PEG/ PSF	Phase inversion method	A glucose assay kit	1.41 mg ISF	10 min	Rat	55

Table 1 *(Contd.)*

Extraction principle	Targets	MN specifications	MN body materials	MN fabrication method	Related equipment	Sampling volume/rate	Sampling time	Test subject	Ref.
Swelling force	ISF	10 × 10 array of HMNs, 600 μm length	PMVE/MA/PEG	Micromolding	Microplate reader	0.84 ± 0.24 mg ISF	1 h	Rat	59
	Theophylline, caffeine and glucose in ISF	19 × 19 array of HMNs, 600 μm length	PMVE/MA/PEG	Micromolding	HPLC, a glucose assay kit	N.R.	N.R.	Rat	60
	Electrolyte ions, glucose, lactate and proteins in ISF	10 × 10 array of HMNs, 1266 ± 91 μm length	PVA/CS	Micromolding	Oxidase-based TMB and potassium iodide mixed solution, chloride assay kit, lactate assay kit, Coomassie Brilliant Blue G-250	1.25 ± 0.37 mg ISF	10 min	Rabbit	61
	Glucose in ISF	10 × 10 array of HMNs, 600–1000 μm length	PVA/PVP	Micromolding	A glucose assay kit	4.4 mg ISF	12 min	Rat	62
	Nucleic acids in ISF	7 × 7 array of HMNs, 550 μm length	PNA/alginate	Micromolding	A fluorescence scanner	6.5 μL ISF	2 min	Human abdominal skin	63
	Protein in ISF	10 × 10 array of HMNs, 800 μm length	PVME/MA/PAA/PEG	UV curing, thermal curing, micromolding	A reversed-phase column	6 μL ISF	10 min	Rat	64
	Glucose and cholesterol in ISF	10 × 10 array of HMNs, 800 μm length	MeHA	UV curing, micromolding	A glucose assay kit, a cholesterol quantitation kit	2.3 ± 0.4 mg ISF	10 min	Rat	66
	Glucose and vancomycin in ISF	11 × 11 array of HMNs, 600 μm length	GelMA	UV-curing, micromolding	A glucose assay kit, the LC-MS/MS system	2.5 mg ISF	10 min	Rat	65
	Urea in ISF	15 × 15 array of HMNs, 387 ± 16 μm length	C-GelMA	Micromolding	Urea assay kits, UV–vis spectroscopy	3.5 ± 0.1 mg ISF	30 min	Agarose gel	67
Iontophoretic	Glucose in ISF	37 PMNs, 250 μm length	PAMPS/PGMA	Micromolding, sacrificial pore-causing agents	An enzymatic biobattery, a glucose assay kit	40 μL	1 h	Pig skin	74
	Glucose in ISF	31.8 needles per cm^2 PMNs, 600 μm length	PGMA	Micromolding, template perforation, sacrificial pore-causing agents	An MN-RI glucose sensor, a FPCB, an MN therapeutic component	N.R.	5 min	Rat	75
	Glucose in ISF	29 SMNs, 2.2 mm length	SS	N.R.	An RI/sensing electrode	1.1 μM ma^{-1} h^{-1}	9 min	Rat	22

Abbreviations: SMN: solid microneedle; N.R.: not reported; HMN: hollow microneedle; DRIE: deep-reactive ion etching; BHF: buffered hydrofluoric acid; SS: stainless steel; PGMA: poly(glycidyl methacrylate); PVF: polyvinyl formal; HA: hyaluronic acid; PDMS: polydimethylsiloxane; EtOH–NaOH: ethanolic sodium hydroxide; PDA: polydopamine; PEG: poly(ethylene glycol); PSF: polysulfone; PMVE/MA: poly(methyl vinyl ether-*alt*-maleic acid); HPLC: high-performance liquid chromatography; PNA: peptide nucleic acid; C-GelMA: cross-linked gelatin methacryloyl; PAA: poly(acrylic acid); LC-MS: liquid chromatography–mass spectrometry; FPCB: flexible printed circuit board; PAMPS: poly-2-acrylamido-2-methylpropane sulfonate; RI: reverse iontophoresis.

bined with a hollow MN. Generally, hollow MNs are relatively brittle and require materials with higher mechanical strength. Therefore, long hollow MNs (>1500 μm long) are usually a single stainless steel needle for blood extraction,[36] but short hollow MNs can be made of various materials (titanium, Si, glass, polymers) and can be arranged into an array for ISF extraction. The elastic chamber made of polydimethylsiloxane (PDMS) is a simple and desirable actuator as negative pressure which can be readily induced by elastic deformation. Li *et al.* presented a vacuum-pressure-aided blood extraction system with a Ni hollow MN for a colorimetric glucose sensor (Fig. 2A).[37] They connected a hollow MN to a PDMS microchamber, which was elastically deformable by a finger push to evacuate the air inside, and the resulting negative pressure drove the blood to the chamber, followed by capillary transport of the blood through a filtering and glucose oxidase (GOx)-immobilized paper channel; glucose levels were detected through colorimetric changes in the paper. Moreover, the control component could be fabricated by the injection-molding of plastics or rubbers such as acrylonitrile butadiene styrene and thermoplastic elastomer. Blicharz *et al.* assembled an MN-based tap-actuated device for painless blood collection, and a solid MN array was used to pierce the skin and induce a vacuum to withdraw blood (Fig. 2B).[25] The device yielded 100 μl of heparinized whole blood by mixing the blood with lithium heparin anticoagulant in the inner microfluidic channel. This device is suitable for most frequently ordered point-of-care testing (POCT).[25] Interestingly, Miller *et al.* described a vacuum-free stainless steel MN with a cylinder concentric substrate for pressure-driven ISF extraction (Fig. 2C).[16] The unique opening design generated a local pressure at the tissue surrounding the insertion point, and consequently transported about 1.5 μL ISF into a single MN without the need for an additional vacuum.

Apart from MN-connected extraction, multiple insertions of solid MN devices also encourage the biofluids to migrate to the skin surface through the micropores, which were then collected *via* vacuum suction or a well-absorbent film for sub-

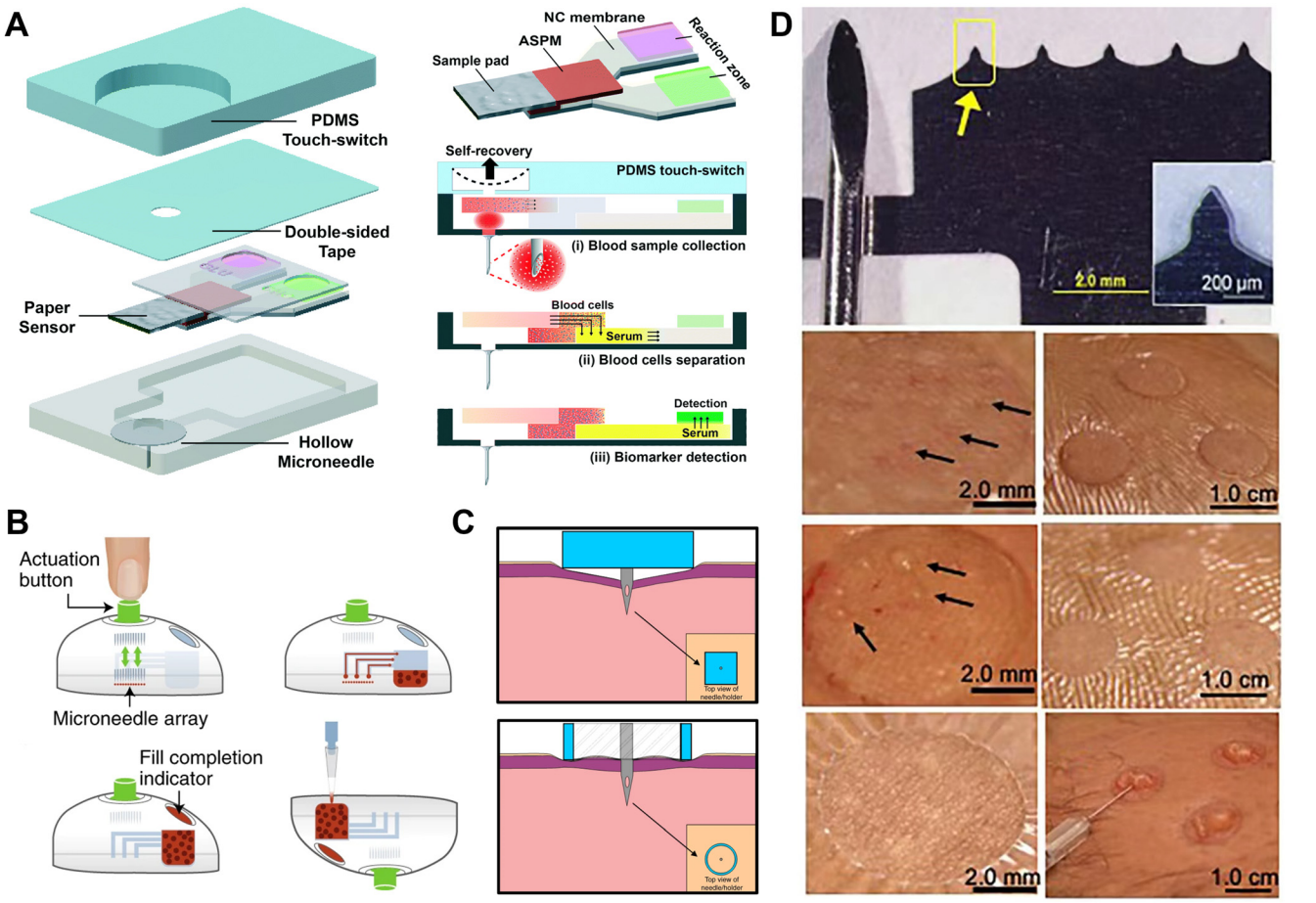

Fig. 2 ISF collection by negative pressure through hollow and solid MNs. (A) A single hollow MN combined with a PDMS switch and a paper-based sensor for one-touch-activated blood multi-diagnosis. Adapted with permission from ref. 37. Copyright 2015, Royal Society of Chemistry. (B) One-step collection of capillary blood samples with a tap device and solid MNs. Adapted with permission from ref. 25. Copyright 2018, Springer Nature. (C) A single hollow MN with planar and cylinder concentric substrates for ISF extraction. Adapted with permission from ref. 16. Copyright 2018, Springer Nature. (D) MN device and ISF collection by MN treatment compared with a suction blister. Adapted with permission from ref. 17. Copyright 2020, American Association for the Advancement of Science.

sequent analysis. Prausnitz's group utilized 700–1500 μm long, glass MNs to penetrate the skin, and ISF was extracted from the generated pores with vacuum pressure.[35] Then 1–10 μL ISF was extracted within 2–10 min for glucose measurements. The same group then utilized 650 μm long stainless steel MNs to press the skin, and then blood-free ISF flowed to the skin surface through the micropores.[38] The ISF was then absorbed through a thin strip of filter paper on the back of the MN patch for subsequent analysis. This method can collect >1 μL ISF within 2 min. Subsequently, they modified the method by applying a vacuum to the pores after the MN had created a pathway for the ISF (Fig. 2D).[17] The vacuum was slowly increased from 0 to −50 kPa over a course of ~3 min, collecting 2.3 ± 2.6 μL clear ISF without visual traces of blood within 20 min. In contrast, the traditional blister method collects ISF from the blister by applying a vacuum at 40 °C for 1 hour, separating the epidermis from the dermis and filling the resulting blister with liquid, which often leads to skin damage, infection and bleeding,[39] and requires a higher sample volume.[19]

Moreover, the pressure gradient can be generated by introducing a higher molecular weight osmolyte into the surrounding ISF. Zheng *et al.* designed osmolyte-powered hydrogel MNs composed of osmolytes (maltose) and high-swelling methacrylated hyaluronic acid (MeHA).[40] During the extraction process, the dissolved osmolytes in the matrix provided an osmotic pressure that increased the diffusion of ISF from the skin to the hydrogel matrix. The MNs extracted 1.96, 3.11, 3.83, and 4.67 μL of ISF in 1, 3, 5, and 10 min, respectively, which were around 1.5-fold those extracted by MeHA MNs. Through the integration with the electrochemical glucose sensors, the whole system permits a rapid quantification of glucose *in vivo*.

2.2. Capillary force-based extraction

Capillary force-based extraction could drive the blood or ISF flow because of the solid–liquid interfacial interaction between two lyophilic solid surfaces (*e.g.*, in the narrow channel in hollow MNs). In general, the sampling rate based on capillarity can be expedited by reducing the contact angle (θ) (Fig. 1), narrowing the microchannel diameter, or inserting a "wick" into the hollow MN.[41] While the inner diameter of a hollow stainless steel MN is often too large (>60 μm) to provide sufficient capillary force, silicon (Si) is mainly used to prepare ultra-fine hollow MNs due to its accurate microfabrication technology, endowing the hollow MNs with self-powered ability based on enhanced capillarity.

Different from extracting blood with a single needle, an MN array requires a certain density and size to extract enough ISF for further analysis. Mukerjee *et al.* pioneered the extraction of ISF from an array of 20 × 20 "volcano-like" hollow MNs (10 μm in hole diameter) on a bulk Si wafer.[42] The extracted ISF took 15–20 min to be transferred to the back of the microfluidic system with the aid of capillary action. Then commercial glucose strips were used to measure glucose concentrations in the collected ISF. However, such an extraction method could cause measurement delays.[42] Strambini *et al.* fabricated a silicon-based MN patch by etching oxidation (Fig. 3A); they

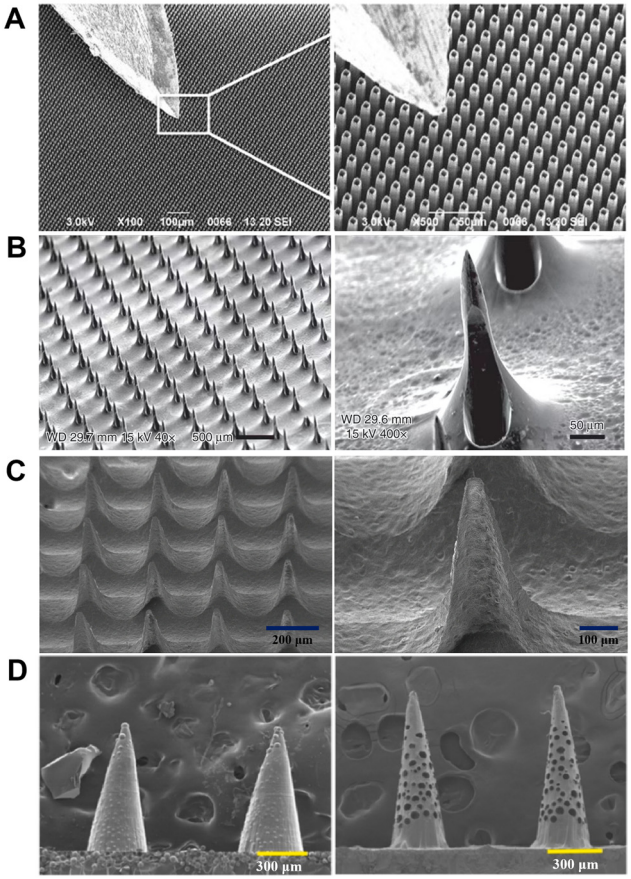

Fig. 3 ISF collection by capillary action through hollow and porous MNs. (A) SEM images of SiO_2 hollow MN arrays with a typical insulin needle sitting on the top for comparison. Adapted with permission from ref. 43. Copyright 2015, Elsevier. (B) SEM images of "snake fang" hollow MNs. Adapted with permission from ref. 44. Copyright 2019, Springer Nature. (C) Characteristics of a sponge-forming MN patch. Adapted with permission from ref. 51. Copyright 2019, Springer Nature. (D) SEM images of MNs embedded with glass microspheres and porous MNs after etching by hydrofluoric acid. Adapted with permission from ref. 52. Copyright 2021, Elsevier.

narrowed the inner diameter of each hollow MN to 4 μm and increased the density to 1×10^6 needles per cm^2 in order to enhance the capillary action.[43] Li *et al.* prepared silicon hollow MNs by a deep-reactive ion etching (DRIE) process, and achieved a tip radius as small as 5 μm (Fig. 3B).[44] Such devices allowed the sensing elements to be integrated either within the needle borehole or on the backside of the device, relying on capillary filling of the borehole with dermal ISF for transporting clinically relevant biomarkers to the sensor sites.[44] Interestingly, Ribet *et al.* developed a minimally delayed intradermal CGM device using a single hollow Si MN-based system, in which an ultra-miniaturized electrochemical sensing probe was integrated into the lumen of the MN, and real-time measurements can be performed entirely on molecular diffusion over a short distance driven by passive capillary lumen filling.[45] In addition to hollow MNs, there are some MNs with grooves on the surface for biofluid extraction[46]

through capillary force. For example, You *et al.* demonstrated a multi-groove MN array integrated with a paper-based glucose sensor.[46] The multi-groove MNs were prepared by a one-step preparation method based on the refraction index variations of poly(ethylene glycol)diacrylate (PEGDA) in the process of photopolymerization. The glucose strip on the substrate could show a color change about 2 min after puncture.

In addition, porous MNs can be considered as a hybrid of solid and hollow MNs. The interconnected porous structure can automatically draw liquid *via* capillary force, and the resulting liquid is then collected by centrifugation for the subsequent analysis of metabolites. As blood passed through the porous structure, blood cells were trapped, leaving only plasma for analysis. For example, Gholami *et al.* fabricated microporous ceramic MNs by the method of centrifugal casting, with adjustable porosity (up to 60%) and interconnected micropores (of diameter ~1–1.5 μm).[47] By extracting glucose in simulative skin, the porous MNs with a higher porosity, interconnection rate and specific surface area demonstrated more accurate glucose detection. Due to the stringent conditions during the manufacturing of a ceramic or metal porous structure,[48] polymers are mainly used to prepare porous MNs owing to the simple micromachining process and low cost; these include poly(glycidyl methacrylate) (PGMA), poly(lactic acid) (PLA), poly(lactic-*co*-glycolic acid) (PLGA), PDMS, cellulose acetate, and so on.[49] For example, sacrificial pore-causing agents or templates are used to create pores in the polymer matrix during the manufacture of porous polymer MN. By using poly(ethylene glycol) (PEG) as a porogen, Liu *et al.* prepared a porous MN array from PGMA which was synthesized by photopolymerization in the presence of a PEG solution.[50] The water absorption speed and mechanical strength can be modulated by varying the ratio of porogen.[50] Chen *et al.* prepared a sponge-forming MN patch composed of polyvinyl formal (PVF) (Fig. 3C); the MNs can extract 3.6 ± 0.6 mg ISF in 5 min and retain their structural integrity without leaving residues in the skin after usage.[51] Zhao's group prepared an aptamer-decorated porous MN array by replicating the negative molds comprising glass microspheres with UV-curable ethoxylated trimethylolpropane triacrylate (ETPTA) (Fig. 3D).[52] The porous MN arrays achieved a significantly increased specific surface area, and thus vast aptamer probes could be immobilized to directly and efficiently capture biomarkers from ISF.

However, porous polymer MNs are physically brittle. One attempt to obtain better mechanical strength is coating a porous structure around the solid MNs. Takeuchi *et al.* conceived a sponge-like porous MN made from hyaluronic acid (HA) coated with a porous PDMS layer.[53] The HA provided sufficient mechanical properties for the MNs in the dry state, and exhibited elastic porous MNs after its rapid dissolution, so that it can absorb fluid by manual compression. Recently, Puttaswamy *et al.* coated porous PLGA on the surface of maltose MNs.[54] The resulting core–shell MNs sustained ten times the force required to penetrate the skin.[54] In addition, considering the poor hydrophilicity and adhesion of porous MNs, which limited the extraction rate of ISF, Liu *et al.* deposited a mixture of polydopamine (PDA) and PEG coating for the hydrophilic and anti-adhesive modification of porous polymer MNs, which can be extended to hydrophobic polymers generally used in medical fields.[55]

2.3. Swelling force-based extraction

Hydrogel MNs, which are rigid in the dry state but swell into a porous structure after liquid absorption, enable both effective skin penetration and biofluid extraction. Since hydrogels contain numerous hydrophilic groups (*e.g.*, $-NH_2$, –OH, and $-SO_3H$),[56] the swelling ability of hydrogel MNs acts like a sponge and can extract ISF without additional force. When in contact with ISF, the hydrogel surface is attacked by solvent molecules and starts expanding, allowing for further molecule penetration into the hydrogel network, until an equilibrium of the swelling and elastic network retraction is reached.[57,58] As with porous MNs, the extracted ISF can be liberated from the hydrogel MNs by centrifugation; however, the structural properties of the hydrogels make the recovery process of target biomarkers time consuming due to a large amount of water within the hydrogel structure. Nevertheless, the fabrication process of hydrogel MNs by mold casting is relatively simple, and they can effectively collect ISF due to the relatively large capacity of the sampling volume.

Prausnitz's group first proposed the use of hydrogel-forming MN arrays for biomarker extraction and analysis by their integration into conventional analytical microtubes and microplates.[59] MN patches were made of cross-linked hydrogel composed of poly(methyl vinyl ether-*alt*-maleic acid) and PEG by micromolding. The MN patches swelled with water up to 50-fold in volume depending on the cross-linking degree, and collected ISF from the skin of rats. Donnelly's group then used the above MN arrays to assess glucose levels in volunteers following oral dosing with glucose powder, indicating their viable application in BG monitoring in patients with diabetes.[60]

Interestingly, He *et al.* recently reported a hydrogel MN patch made of polyvinyl alcohol (PVA) and chitosan (CS).[61] After insertion to rabbit skin for 10 min, the MN patch can extract 1.25 ± 0.37 mg ISF. Meanwhile, the thermal degradation of PVA facilitated the recovery of target biomarkers from the MN array. In addition, PVA is also used with polyvinylpyrrolidone (PVP) to improve the overall swelling property of MN patches, thus allowing the MN patches to extract ISF more efficiently. For example, Xu *et al.* prepared a PVA/PVP MN patch that was able to extract 4.4 mg ISF within 12 min and recover ISF by mild heating.[62] Al Sulaiman *et al.* developed an MN patch coated with an alginate–peptide nucleic acid hybrid material for the sequence-specific sampling and isolation of biomarkers, which can extract ~6.5 μL ISF within 2 min.[63] Recently, Laszlo *et al.* utilized superabsorbent acrylate-based hydrogels to prepare an MN patch that successfully extracted 6 μL of ISF within 10 min.[64]

At present, cross-linked hydrogel made of MeHA or gelatin methacryloyl (GelMA) shows a shorter absorption time and greater swelling ratio.[65,66] The extraction ability is highly

dependent on the concentration of monomer and the polymerization time. Chang *et al.* developed an MN patch using MeHA, which can extract 2.3 ± 0.4 mg of ISF in 10 min (Fig. 4A).[66] More importantly, the extracted ISF metabolites can be efficiently recovered from the MN patches by centrifugation for the subsequent analysis of metabolites such as glucose and cholesterol.[66] Zhu *et al.* prepared GelMA MN patches with various crosslinking degrees and initial polymer concentrations; by tuning these parameters, the swelling (293%–423%) and other mechanical properties of the MN were optimized for the rapid extraction of ISF, and then glucose and vancomycin were quantitatively detected in ISF in an *in vivo* study.[65] Fonseca *et al.* constructed cross-linked GelMA MN patches to extract and detect urea levels in ISF.[67] The MN patches were able to extract 3.5 ± 0.1 mg ISF from the agarose system in 30 min.

Recently, our group developed a dual-responsive hydrogel for the visual detection of glucose (Fig. 4B).[68] The hydrogels were synthesized based on GelMA, pH-responsive nanogel and GOx. The changes of the size and fluorescence intensity of the hydrogel system in response to glucose allowed a quantitative readout of glucose levels in solution and in diabetic mice.[68] Subsequently, we integrated the responsive hydrogel system into MNs, combined with a transparent photocurable resin substrate (Fig. 4C).[69] When applied on the skin of mice, the MNs can respond rapidly and sensitively to the glucose concentration in diabetic mice within 3–5 seconds, and quantitative characterizations of glucose concentrations were achieved through the change of MN height and expansion rate.

2.4. Iontophoresis-based extraction

Iontophoretic transport consists of the electroosmotic flow (EOF) of the solvent as well as the electrophoresis of the charged molecules themselves. Iontophoresis can employ a continuous mild current to promote charged therapeutic agents across the skin layer and even into the systemic circulation and thus significantly facilitates the transdermal delivery of the drugs.[70,71] In contrast, the use of reverse iontophoresis (RI) can electrically draw molecules (*e.g.*, glucose, urea, alcohol, *etc.*) through the epidermis to the skin surface, and then these molecules can be measured *via* electrochemical sensors.[21,72]

GlucoWatch® biographer (Cygnus Inc.) was the first U.S Food and Drug Administration (FDA) approved non-invasive glucose monitor that electrochemically measured the glucose concentrations in skin ISF extracted by RI. RI was carried out by applying a mild current with two skin-worn electrodes to induce ion migration across the skin.[73] However, GlucoWatch® was eventually withdrawn from the market due to the skin irritation caused by the RI process, the long warm-up time (2–3 hours), as well as the need for calibration using standard BG strips. To this end, Joseph Wang and coworkers demonstrated a wearable sensing platform prepared by a screen-printed electrochemical path.[21] The platform achieved

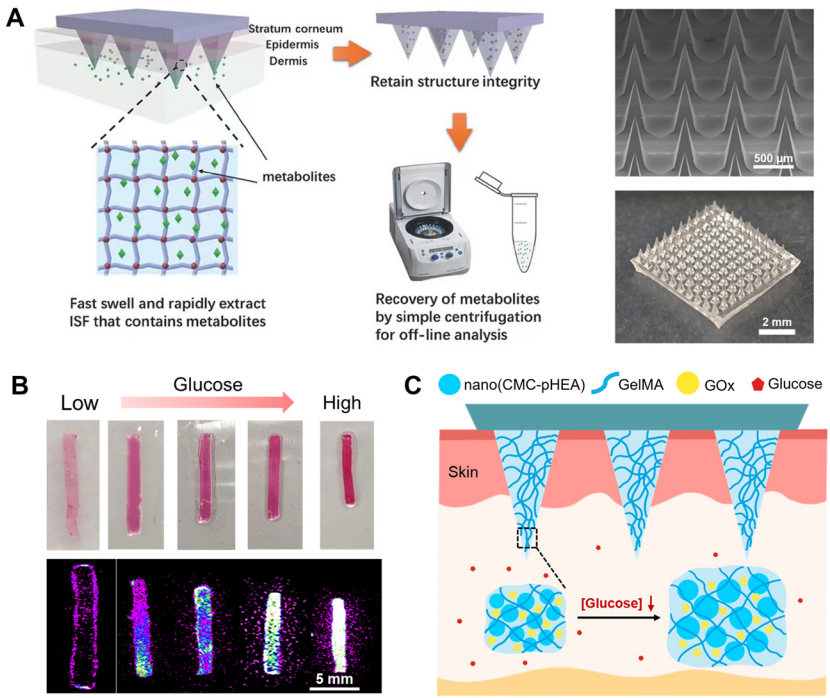

Fig. 4 ISF collection by diffusion into hydrogel MNs. (A) Schematic representation of the rapid extraction of ISF by crosslinked MeHA MN patches. The right panel includes an SEM image and overall photograph of an MeHA MN patch. Adapted with permission from ref. 66. Copyright 2017, Wiley-VCH. (B) *In vitro* glucose sensing by GelMA/CMC-pHEA hydrogels, including optical and fluorescence images, respectively. Adapted with permission from ref. 68. Copyright 2019, Elsevier. (C) Schematic illustration and responsive mechanism of an MN patch made by the hydrogels in (B) for glucose monitoring. Adapted with permission from ref. 69. Copyright 2023, Elsevier.

simultaneous noninvasive sampling and analysis of two different biofluids. With sweat stimulation by transdermal pilocarpine delivery at the anode, alongside the extraction of ISF by RI at the cathode, the panda-looking tattoo patches can detect real-time reliable changes in sweat-alcohol and ISF-glucose.[21] This platform is shown to be extremely attractive for next-generation epidermal biosensing systems using RI.

Nevertheless, the barrier function of the stratum corneum limits the formation of stable transdermal currents, and only small molecules can be the candidates for transdermal delivery and collection.[70] Therefore, other researchers combined MNs with RI or iontophoresis to lower the transdermal resistance and transport larger molecules. This technology has been used to enhance ISF extraction and electronically controlled insulin delivery.[22,72,74,75] For example, Kusama *et al.* report the application of ion-conductive porous PGMA MNs for improving iontophoresis.[74] The porous MN-generated EOF greatly enhanced the transdermal molecular extraction, similarly to the flow induced by external pressure. This design enhanced the efficiency of the EOF-assisted delivery of a model drug (dextran) and the extraction of glucose in pig skin. Furthermore, an enzymatic biobattery (fructose/O_2 battery) can serve as the integrated power source to drive the EOF-assisted transdermal iontophoresis, showing the possibility of EOF-based wearable MN patches in the future. Meanwhile, Xie's group presented an integrated wearable closed-loop system (IWCS) based on a mesoporous MN array for diabetes diagnosis and treatment (Fig. 5A).[75] The IWCS consisted of an MN glucose sensor based on MN-RI extraction and electrochemical sensing, a flexible printed circuit board (FPCB) as an integrated recording and control section, and a therapeutic component (MN-iontophoretic insulin delivery by an electrical trigger). After the mesoporous MNs pierced the skin, the glucose in the ISF was extracted into the chamber *via* RI, followed by detection *via* electrodes. Accordingly, the overall system can release insulin to regulate hyperglycemia in a

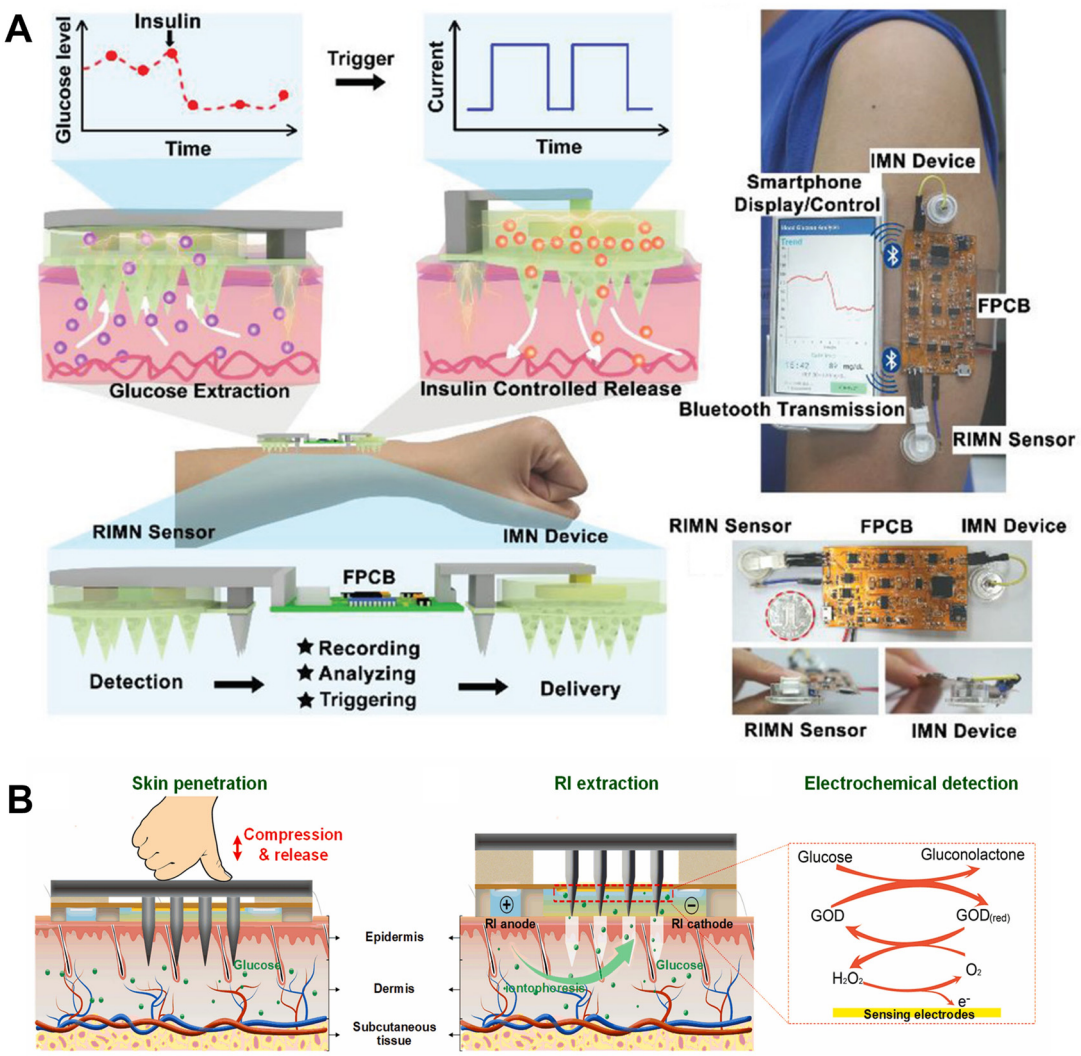

Fig. 5 ISF collection by iontophoresis through porous and solid MNs. (A) A closed-loop system based on mesoporous MN-RI for diabetes treatment. Adapted with permission from ref. 75. Copyright 2021, Wiley-VCH. (B) A touch-actuated glucose sensor fully integrated with solid MNs and RI for diabetes monitoring. Adapted with permission from ref. 22. Copyright 2022, Elsevier.

timely and intelligent manner, which makes it a promising platform to improve the treatment efficiency. Subsequently, the same group developed a touch-actuated glucose sensor by effectively integrating a solid MN array, an RI sampling unit, and a glucose electrochemical sensing unit (Fig. 5B).[22] The solid MNs created uniform microchannels in touch-actuated piercing and self-retraction mode, coupled with iontophoresis which significantly enhanced the sampling efficiency and consistency for ISF glucose. They further developed a smartphone-based glucose electrochemical detection platform, making it suitable for home care diabetic monitoring.

As discussed above, MNs as biofluid collectors have been widely investigated for *in vitro* diagnostic systems. However, sampling ISF using an MN-based system involves a complex process, and most previous studies are limited by submicroliter sampling volumes and poor correlation of the measurement of biomarkers.

It is reported that ISF extraction critically depends on the transport mechanism, and an ideal ISF sampling system should reliably sample ≥1 μL of ISF in ≤20 min,[34] which is sufficient for multiple analytical assays and is without tissue damage or irritation. The rank order of the ISF amount collected by MNs is as follows: hydrogel MN (0.0030 pL per MN (12 h insertion)) < paper-based porous MN (0.0033 pL per MN (20 min insertion)) < hollow MN (0.01–0.03 pL per MN (20 min insertion)).[34] Accordingly, hollow MNs enable a sufficient extraction of ISF, while the sampling rate of porous MNs is limited by diffusion through the dermis. However, the porous MNs provide advantages such as their applicability for biodegradable materials and the simple fabrication and assembly with microfluidic systems, whereas the hollow MNs are generally made of non-biocompatible materials and fabricated by a complex process which limits the microfluidic system design. It seemed that ISF extraction by swelling force was not satisfactory. Actually, the extraction amount of ISF had a considerable relationship with the properties of the material itself rather than the swelling force method itself. Therefore, it was important to exploit the materials with good swelling properties.

Moreover, the pressure gradient across the skin layer can collect a significant amount of ISF in a short period of time compared with the other techniques. The applied vacuum can provide a stable pressure gradient over a long period of time. In addition, pressure differentials can also be generated by introducing high molecular weight penetrants with low diffusivity into the surrounding ISF. However, the tolerance of the skin to pressure needs to be optimized, and progressive pressure can result in much less skin damage. In addition, many issues have not been fully studied, and further research is required to unlock the maximum potential of MN-based biosensors.

3. Integrated MN sensing systems

In the above investigations, ISF was first collected by the MN device, and then most of the samples were analyzed in instruments separately, which required an additional transfer step of ISF. To meet the requirements for POCT or home testing, MNs have been integrated with other devices or smart materials for the direct extraction of biomarkers, rapid testing, and easy readout.[76] Generally, glucose biosensors rely on the monitoring of the oxygen consumption or the chemical products during the enzyme-catalyzed reaction (eqn (1)).

$$\text{Glucose} + O_2 \xrightarrow{\text{glucose oxidase}} \text{gluconic acid} + H_2O_2 \quad (1)$$

In this section, we summarize the recent reports emphasizing the different glucose-sensing principles of MN systems, including the surface-enhanced Raman scattering (SERS) method, colorimetric method, and fluorescence method (Table 2), whereas the electrochemical glucose-sensing mechanism, which is most widely used in diabetes monitoring, will be emphasized in section 4 separately.

3.1. SERS-based MN glucose sensors

Raman spectroscopy is a spectroscopic technique providing more specific chemical information and unique vibrational signatures of target biomolecules compared with mid- or near-infrared spectroscopy.[77] However, the Raman signal is intrinsically weak when measuring dermal components deeper than 700 μm, and the detection sensitivity is reduced by the small Raman scattering cross-section (10^{-29}–10^{-32} cm^2) of endogenous biomolecules, which limits its application in biosensing. Fortunately, SERS effectively overcomes this weakness due to the dramatic enhancement of Raman signals by plasmonic effects.[78,79]

Combined with MNs, SERS has been used for the *in situ* detection of glucose,[80–83] pH,[84] redox potential,[85] drug concentration and bacteria[86] in a painless, effective, and minimally invasive approach, and the resulting signal is subsequently enhanced by metal nanoparticles (NPs). Initially, Liu and coworkers first proposed using MNs as a tool to solve the limitation of Raman transmission depth in the skin.[80] They proposed an Ag-coated stainless steel MN-based SERS probe for the sensitive detection of rhodamine 6G (R6G) and glucose at a depth of more than 700 μm in simulative skin. This work showed the potential of using MN for SERS measurements and achieved larger penetration depths with augmented signals. However, the use of stainless steel MNs caused a strong skin immune response. To solve this problem, the same group subsequently designed a hollow agarose MN coated with a silver layer for the SERS detection of glucose molecules.[81] The agarose materials were more biocompatible than stainless steel even if the MN was broken inside the skin. Even with a slightly reduced measurement accuracy, the Ag-coated agarose MN still quantified glucose inside the skin phantoms with a wide range from 5 to 150 mM within 10 s. Unfortunately, Ag-coated agarose MNs were not used to demonstrate direct intradermal measurements *in vivo*. To promote the application of Raman–MN technology for *in situ* measurements of glucose, the same group developed a novel sensor based on a poly(methyl methacrylate) (PMMA) MN array (Fig. 6).[83] The

Table 2 Comparison of performance of different MN glucose sensors

Principle	Targets	Sensing mechanism	Microneedle specifications	Detection ranges	Time consumptions	Ref.
SERS	Glucose	N.R.	Ag-coated SS HMNs	5–150 mM	N.R.	80
	Glucose	1-DT	Ag-coated agarose HMNs	5–150 mM	10 s	81
	Redox, pH	AQ, 4-MBA	SS SMN with GNSs	N.R.	5 min	85
	R6G	A thin strip of filter paper fixed with PSS coated with AuNRs	SS SMNs	N.R.	5 min	82
	pH	4-MBA	Polymer MN coated with AuNRs	5–9 for pH	N.R.	84
	Glucose	1-DT	Ag-coated PMMA MNs	0–20 mM	15 min	83
	E. coli	Specific aptamer towards *E. coli*	GNpops-coated polymer MNs	LOD: 143 CFU per g	3 min	86
Colorimetry	Electrolyte ions, glucose, lactate, proteins	Oxidase-based TMB and potassium iodide mixed solution, chloride assay kit, lactate assay kit, Coomassie Brilliant Blue G-250	PVA/CS MNs	0–16 mM for glucose, 20–40 mM for chloride, 5–30 mM for lactate, 28–194 mM for BSA	1 min	61
	Glucose, cholesterol	Oxidase-based MADB TOPS colorimetric systems	SS MNs with a paper-based multiplex sensor	0–15 mM for glucose, 0–17.8 mM for cholesterol	3 min	37
	Glucose	GOx-based TMB-HRP	Photopolymer MNs with a colorimetric paper-based backplate	0.1–10 mM	30 s	89
	Glucose, lactate, cholesterol, pH	Oxidases/HRP/three chromogenic dyes systems, the pH indicator bromocresol green	HA-MeHA MNs with a sensing-reagent-decorated test paper	0–16 mM for glucose, 0–3.2 mM for lactate, 0–12 mM for cholesterol, 5–8 for pH	11 min	92
	Glucose	GOx-based TMB-HRP	PVA MNs with a colorimetric layer	2.8–22.3 mM	10 min	94
	Glucose	GOx-MnO_2@GO based TMB	GelMA MNs with a GOx-MnO_2@GO base and a patch for glucose-biosensing	2.8–16.7 mM	5 min	95
	pH, glucose, uric acid, temperature	pH indicators, GOx/uricase-based TMB-HRP colorimetric systems, and temperature-responsive solutions	HA MNs	6–8 for pH, 1–10 mM for glucose, 0.2–1.6 mM for uric acid, 36–39 °C for temperature	10 min	91
	Glucose	FPBA-based colloidal crystal colorimetric systems	Resin SMNs coated with colloidal crystals	5.6–22.3 mM	5 min	90
	pH, glucose, histamine	PAM/FPBA/histamine aptamer-based colloidal crystal colorimetric systems	PEGDA and AM MNs with colloidal crystals	LOD: 8 for pH, 1 mg mL^{-1} for glucose, 2 μg mL^{-1} for histamine	30 min	101
Fluorescence	Glucose	Fluorescently labeled *E. coli* GBP	SS SMNs	3–40 mM	30 s	107
	Glucose, ATP, L-tyrosinamide, thrombin	Fluorescently labeled aptamer probe	MeHA HMNs	LOD: 1.1 mM for glucose, 0.1 mM for ATP, 3.5 μM for L-tyrosinamide, and 25 nM for thrombin	2 min	104
	Glucose	PBA functionalized hydrogel with fluorescent nanodiamonds	Nanodiamond-based boronic HMN	0–36.1 mM	N.R.	108
	Glucose	Diboronic acid and anthracene functionalized hydrogel	Silk MNs	2.778–25 mM	15–20 min	109

Abbreviation: N.R.: not reported; LOD: limit of detection; SMN: solid microneedle; HMN: hollow microneedle; SS: stainless steel; PSS: poly(styrenesulfonate); AuNRs: gold nanorods; R6G: Rhodamine 6G; 4-MBA: 4-mercaptobenzoic acid; PMMA: poly(methyl methacrylate); 1-DT: 1-decanethiol; MB: methylene blue; *E. coli*: *Escherichia coli*; GNpops: gold nanopopcorns; TMB:tetramethylbenzidine; GNSs: gold nanoshells; PAM: polyacrylamide; AQ: anthraquinone-2-carboxylic acid; FPBA: fluorophenylboronic acid; PBA: phenylboronic acid; GBP: glucose-binding protein; ATP: adenosine triphosphate.

high light transmission of PMMA enabled laser light as well as Raman signals to transmit through the MN, and the PMMA MN was coated with a thin silver film to enhance the Raman signals. After being modified with the glucose capture agent of 1-decanethiol (1-DT), the functional MN array achieved intradermal measurements of ISF glucose in diabetic mice.

However, during the MN insertion into the skin, the plasmonically enhanced substrate may undergo biological contamination and lose activity, therefore impeding the performance of SERS-integrated MN arrays.[87] To this end, Prausnitz's group invented a plasmonic paper by immobilizing poly(styrenesulfonate) (PSS)-coated gold nanorods (Au NRs) on a thin strip of filter paper using plasmonic calligraphy.[82] The

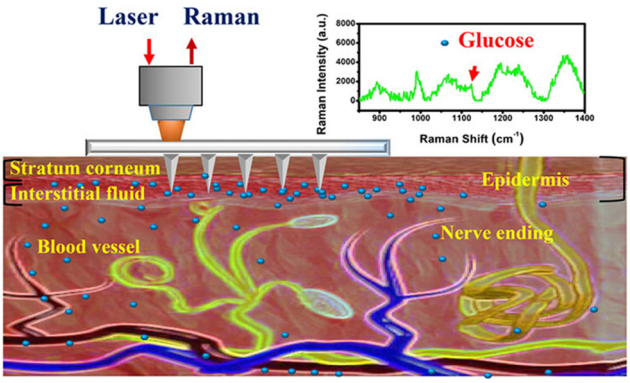

Fig. 6 Schematic illustration of a PMMA MN array using SERS methods for the transdermal detection of glucose. Adapted with permission from ref. 83. Copyright 2020, American Chemical Society.

MNs collected ISF onto the plasmonic paper on the patch backing, and then SERS spectra were obtained to detect and quantify the R6G bound on the Au NRs. The plasmonic paper paved the way for the integration of SERS-based detection with MN arrays and wearable devices. Nevertheless, it took a long extraction time for the small volume of ISF collected by the stainless steel MNs to flow through the whole MN patch and then spread into the paper reservoirs. Recently, Hsieh *et al.* prepared a hydrogel MN patch that can extract sufficient ISF rapidly, and then the ISF in the needles can be recovered into a moist cellulose paper through spontaneous diffusion.[88] The paper can be functionalized with a plasmonic array or enzymatic colorimetric reagents, enabling a desired detection capacity. The authors functionalized the cellulose paper with Au nanoparticles (AuNPs) to serve as an ultrasensitive, label-free SERS sensing platform.[88] The excellent molecular fingerprinting ability through a portable 785 nm Raman spectrometer enabled the robust identification of various medications and drugs in the ISF, even at ultralow concentrations (sub-ppb level). This MN-assisted paper-based sensing system allowed a rapid (<30 min), pain-free, minimally invasive monitoring of biomolecules and drugs. Besides, the authors also demonstrated the use of paper for colorimetric analysis.[88] They preloaded the cellulose paper with specific oxidases and dye reagents, according to the nature of the target biomolecule. Then, the color readout would be in response to the target concentration, allowing rapid determination by the naked eye.[88]

In brief, the Raman–MN technology passed its hurdle for the *in vivo* detection of glucose, and the MN array-based SERS biosensor has the potential to be developed for a new painless wearable glucose detection instrument in the future.

3.2. Colorimetric MN glucose sensors

Based on the merits of easy fabrication, portability, cost effectiveness and visual readout, colorimetric approaches enable a qualitative and quantitative analysis, and are widely applied in a wide range of POCT devices. Colorimetric data can be directly distinguished with the naked eye, or captured by a smartphone camera, and finally analyzed through RGB value processing for further quantitative analysis. The integration of MN patches with colorimetric methods enables a highly efficient extraction of biomarkers in ISF and rapid POCT. Colorimetric signals are induced by changes in the chemical structures, densities, orientations, morphologies, or sizes of chromogenic agents during the interaction with the target substance. Based on different principles of color development, the chromogenic agents could be classified as redox-responsive agents[89] and nanostructures.[90–92]

In terms of redox-responsive agents for colorimetric readouts, glucose can be firstly oxidized with a specific oxidase (such as GOx) to generate hydrogen peroxide (H_2O_2), which could subsequently react with a H_2O_2-responsive chromogenic agent (*e.g.*, iodide solution, horseradish peroxidase (HRP)). For example, He *et al.* fabricated a PVA/CS hydrogel MN patch and realized a visual detection of electrolyte ions, glucose, lactate, and proteins in a chromogenic reagent (Fig. 7A).[61] Upon the quick dissolving of the PVA at high temperature, the centrifugation-free recovery of analytes from MNs was easily realized within ~15 min; then, the analytes were detected according to the color reaction between the ISF and the chromogenic reagent of potassium iodide. This method enabled the detection of various health-related biomarkers. However, due to its complicated manual operation, this analysis procedure should be further simplified for health management at home by nonprofessionals.

The paper substrate offers capillary action due to its pore-rich structure, enabling the sample to spread throughout the analysis area, and the huge surface area can be an ideal matrix medium for fixing macro-molecules such as enzymes. Therefore, colorimetric assays on paper are commonly used after ISF extraction by MNs owing to the advantages of hydrophilicity, portability, and cost effectiveness.[37,89] For example, Li *et al.* designed a paper-mediated colorimetric MN system to realize the dual identification of glucose and cholesterol levels in rabbits (Fig. 2A).[37] Blood was collected *via* a single hollow MN. Glucose and cholesterol were oxidized by GOx and cholesterol oxidase on paper, and finally reacted with *N*-ethyl-*N*-sulfopropyl-M-toluidine (TOPS) and *N*,*N*-bis(4-sulfobutyl)-3,5-dimethylaniline disodium salt (MADB) to form purple and green colors, respectively.[37] Callan *et al.* designed a hollow MN device with a colorimetry paper backboard containing a GOx, HRP and tetramethylbenzidine (TMB) enzyme/dye combination.[89] The device rapidly extracted the simulated ISF within 5 seconds, and produced glucose concentration-dependent color changes within 30 seconds.[89] The naked eye can distinguish glucose concentrations in the range of normal (4–7 mM) and hyperglycemia (>7 mM).[89] Similarly, Lee *et al.* designed a porous MN patch with a paper matrix for glucose detection.[93] The absorbed ISF flew through the porous MN and reached the sensor layer due to capillary action. GOx loaded on the sensor layer reacted with ISF glucose to produce H_2O_2, which oxidized the TMB dye and showed blue color development. Recently, Zhu *et al.* demonstrated a colorimetric MN patch for the transdermal detection of multiple metab-

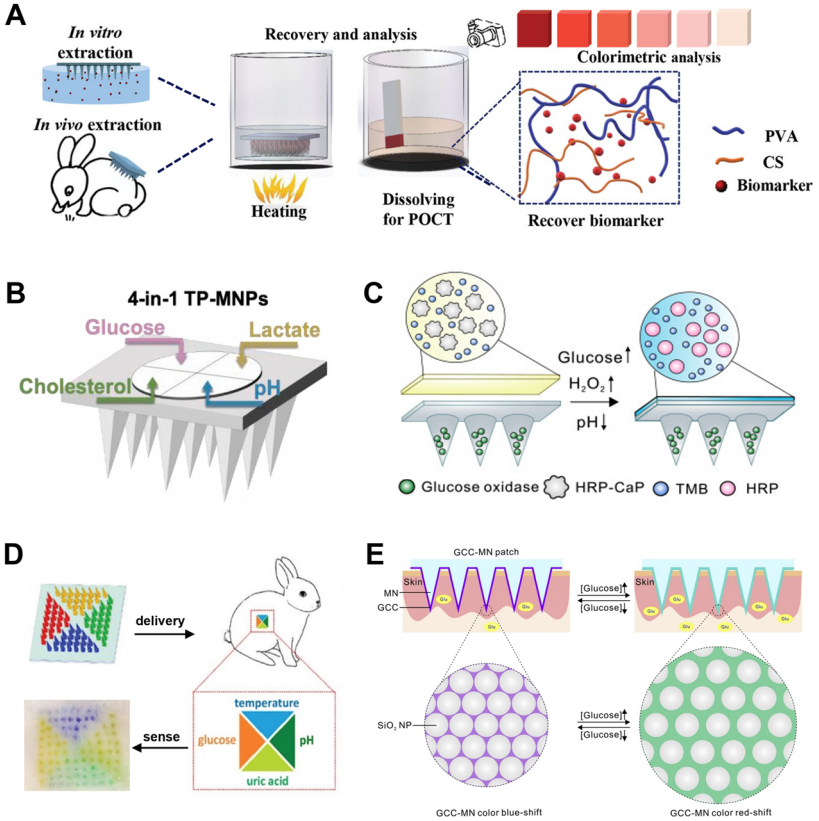

Fig. 7 MN arrays using colorimetric methods for transdermal glucose monitoring. (A) Extraction and recovery of target biomarkers from PVA/CS MNs, and detection of biomarkers using the colorimetric method. Adapted with permission from ref. 61. Copyright 2020, Wiley-VCH. (B) Schematic illustration of the test-paper upon MN patches for the detection of four biomarkers. Adapted with permission from ref. 92. Copyright 2022, Elsevier. (C) Schematic of an all-in-one sampling and display colorimetric MN patch. Adapted with permission from ref. 94. Copyright 2020, Elsevier. (D) Simultaneous detection of four biomarkers *in vivo* using colorimetric dermal tattoo biosensors. Adapted with permission from ref. 91. Copyright 2021, Wiley-VCH. (E) Schematic illustration of the mechanism of a glucose-responsive colloidal crystal-modified MN patch for naked-eye monitoring of glucose concentrations. Adapted with permission from ref. 90. Copyright 2020, Elsevier.

olites, including glucose, lactate, and cholesterol, and pH (Fig. 7B).[92] A highly swellable MN was used to rapidly extract ISF, and then a wax-patterned and sensing-reagent-decorated test paper was combined to achieve the multiplexed colorimetric detection of metabolites on the base of the MN patch.[92]

In addition to producing color on paper located upon MNs, different colors can be directly induced on the MN patch or even on the skin surface. For example, Gu and coworkers developed an transdermal colorimetric MN patch for the all-in-one sampling and displaying of glucose in ISF (Fig. 7C).[94] The PVA-based MN patch consisted of two layers: a GOx-embedded bottom needle layer, and calcium phosphate-encapsulated HRP as well as TMB-immobilized upper layer. The back of the patch turned blue once it met with glucose, and glucose levels in type 1 diabetic mice were quantified by scanning the color intensity of the MN back with a miniaturized scanner.[94] Yang *et al.* developed an MN patch made of GOx-conjugated MnO_2/graphene oxide nanozymes (GOx-MnO_2@GO) and GelMA.[95] ISF immediately diffused into the MNs by the hydro-affinity of the hydrogel to produce H_2O_2, which bound to MnO_2 and promoted the oxidation of TMB on the patch, causing a color change in the MN patch from colorless to blue in hyperglycemia.[95] Besides MN-based sampling, the MN-based injection of diagnostic agents into skin ISF gained great success for the simultaneous multiplexed detection of biomarkers *in vivo* (Fig. 7D).[91] However, this colorimetric sensor only realized a semiquantitative detection due to the low sensitivity and accuracy, and moreover, the safety of dermal tattoos is a controversial issue due to the leakage of dye molecules and H_2O_2 into the skin.

However, many of the above colorimetric systems based on redox reactions contained enzymes and chromogenic substrates, which can cause problems including enzyme denaturation, color quenching, byproduct toxicity, and non-reusability, while nanostructure-based colorimetric agents have recently attracted emerging attention for biomarker sensing.[96] Among them, photonic crystals (PCs) are periodically arranged optical materials,[97] and structural colors result when the lattice constant of PCs is smaller than or comparable to the wavelength of visible light (400–800 nm). Featuring fascinating structural colors, PCs can be mixed with stimulus-responsive hydrogels, where the swelling or shrinking of the hydrogel with the stimulus would lead to a shift in the spectrum or even a visual change in the structural colors. These properties make the PC-

integrated hydrogels promising as biosensors and other tunable optical devices.

To date, several glucose-sensing PCs have been developed in the form of implantable hydrogels, hydrogel dressings, contact lenses, MNs, *etc*. Phenylboronic acid (PBA) was widely used to form glucose-responsive hydrogels. PBA and its derivatives have the capability of reversibly binding with glucose. When combined with glucose, the anionic charged forms of PBA increase, resulting in swelling of the hydrogels.[98] Crystalline colloidal arrays of highly charged monodisperse polystyrene nanospheres were immersed with a PBA-modified hydrogel matrix for glucose monitoring.[99] PCs were also combined with smart contact lenses to measure glucose concentrations in tears. For instance, Elsherif *et al.* prepared a photonic microstructure on a hydrogel film functionalized with PBA.[100] The glucose concentration in tears could be measured with a sensitivity of 12 nm mM^{-1} within a concentration range of 0–50 mM. Gu *et al.* constructed colloidal crystals on the shell of rigid resin MNs for the visualization of glucose (Fig. 7E), where periodic nanostructures (SiO_2 NPs) were encapsulated into a glucose-responsive fluorophenylboronic acid (FPBA) matrix.[90] Once in contact with ISF, glucose entered the FPBA-SiO_2 colloidal crystals, and the expansion of FPBA increased the distance between periodically arranged SiO_2 NPs, resulting in a redshift of MNs from blue to green. This MN patch with a glucose-relevant color display has broad applications in glucose monitoring in POCT. Very recently, Zhao *et al.* prepared structural color MN arrays with different modules to detect three typical wound biomarkers simultaneously, namely pH, glucose, and histamine.[101] FPBA-based hydrogel was added into the MN material to realize the reversible detection of glucose, and the MNs showed a satisfactory spectrum change upon glucose variation.[101]

Nevertheless, these PC-based sensors developed so far require a long reaction time as it often takes tens of minutes or even hours to reach an equilibrium response, due to the relatively long diffusion distance of glucose molecules into the hydrogels. After a stringent process containing template fabrication, monomer infiltration, polymerization, and the etching process, reverse opal PCs were also available for glucose sensing with the assistance of glucose-responsive polymers.[102] Reverse opal PCs have interlinked voids to facilitate the diffusion of the analyte, but still exhibit slow kinetics and hysteresis as the voids are occupied as the gel expands. Therefore, Cai *et al.* reported probes of glucose-sensing photonic nanochains (PNCs), which were capable of continuously and reversibly changing their structural color with glucose within a few seconds, due to the significantly reduced diffusion length to the analyte of glucose.[103] The developed polymerization technology may also provide an effective route to fabricate functional polymer-based hybrid nanostructures.

3.3. Fluorescence-based MN glucose sensors

Fluorescence detection has been extensively explored in disease diagnosis due to its high sensitivity and visual display. Molecules that selectively recognize or interact with targets can be attached to fluorescent probes to realize a sandwich assay. Common target recognition techniques include nucleic acid hybridization,[63] aptamer–target interaction[52,104] antigen–antibody reaction,[31,33] *etc*. The effective integration of fluorescence detection and MNs can provide a sensitive and selective sensing platform to obtain valuable physiological information from ISF in a minimally invasive and painless manner. The main function of MNs in a fluorescence-based sensing system is to participate in the capture and enrichment of the target in ISF, and therefore MNs with good ISF extraction ability are often used for coupling with fluorescence-sensing systems.

Zhao and coworkers presented MNs integrated with PC barcodes for the multiplex detection of three inflammatory cytokines (tumor necrosis factor-alpha (TNF-α), interleukin-1β (IL-1β), and IL-6) in ISF.[31] These probe-decorated PC barcodes allow MNs to capture three different cytokines simultaneously, and fluorescent-tagged antibody can identify these biomarkers immobilized in MNs specifically. The relative content of biomarkers can be read through the fluorescence intensity of the barcodes; meanwhile, the species of these biomarkers can be clearly distinguished by the reflection peaks of the PC barcodes. Recently, Wang *et al.* described a polystyrene MN-based *in vivo* sampling and subsequent on-needle analysis for the ultrasensitive and quantitative measurement of target protein biomarkers in ISF.[33] Capture antibodies were coated onto the surface of MNs for the direct capture of protein biomarkers. Moreover, the quantification sensitivity was significantly increased because of the use of an ultrabright fluorescent plasmonic fluorophore instead of a conventional fluorophore. Immunoassay procedures can be implemented on the double-layer MNs directly, so minimally invasive collection and ultrasensitive protein analysis platforms have been employed in on-the-spot field detection to facilitate rapid disease diagnosis.

Moreover, ligand-specific periplasmic binding proteins as optical biosensors for measuring glucose have been explored for noninvasive sensing, as well as sensing in clinically relevant ranges. For example, *E. coli* glucose-binding protein (GBP) can be used as an optical biosensor when a polarity-sensitive fluorescent probe, acrylodan (Acr), was attached to a cysteine mutation site responsive to glucose binding.[105,106] In the presence of micromolar glucose concentrations, the emission of the bound Acr (510 nm) was quenched and a spectrophotometer was used to observe the glucose-associated fluorescence changes. Due to its high selectivity and specificity for glucose, Brown *et al.* utilized stainless steel MNs to extract the ISF, and then the samples were measured by a L255C mutant of the *E. coli* GBP with an attached fluorescent probe.[107] The micromolar sensitivity of the biosensor reduced the ISF volume required for glucose analysis and minimized the time required for MN application (30 s).

MNs functionalized with antibodies and aptamers have been recently reported for the specific capture of target biomarkers in ISF, followed by *ex vivo* analysis.[33,52] Although these MN devices allowed for on-needle biomarker detection in ISF, the sensors still needed postprocessing steps, such as washing and adding detection reagents, to detect targets of

interest. Zheng *et al.* reported an MeHA hollow MN biosensor based on a fluorescently labeled aptamer probe for the on-needle and reagentless capture and detection of any biomarkers of interest (Fig. 8A).[104] They employed a strand displacement strategy where fluorophore-conjugated aptamers were hybridized with a DNA competitor strand conjugated to a quencher molecule. Rapid measurements (2 min) of glucose, adenosine triphosphate, L-tyrosinamide, and thrombin were demonstrated *in vitro*. Moreover, this assay enabled an accurate and sensitive quantification of rising and falling concentrations of glucose in an animal model of diabetes, especially in the severe hypoglycemia range, which cannot be detected using commercially available glucose-monitoring devices.[104]

Furthermore, due to the strong photostability and biocompatibility of fluorescent nanodiamonds, Zhang *et al.* integrated them into the FPBA-functionalized hydrogel, which can generate fluorescent signals in response to environmental glucose concentrations (Fig. 8B).[108] Furthermore, they designed and successfully loaded the hydrogel system into MNs with a porous hollow structure by porogen leaching technology.[108] The porous structure can effectively enhance the extraction of ISF by capillary action, reducing the lag time and facilitating glucose monitoring *in vivo*. The device demonstrated remarkable long-term photo- and signal stability *in vivo* with both small and large animal models. This study presents a new strategy of fluorescence-based CGM toward the treatment and control of diabetes. Similarly, Sang *et al.* presented a bioresorbable MN array for CGM, which can reversibly express fluorescence intensity according to glucose concentration by using a glucose-responsive fluorescent monomer (GF-monomer).[109] The MNs consisted of two layers: a needle layer made of silk, which contained a GF-monomer; and a PVA backing layer. The GF-monomer was composed of a diboronic acid moiety, which was a recognition site that bound to glucose, and an anthracene moiety that emitted fluorescence. After attaching the sensor to the human body, illumination of the MN sensor with an excitation light (405 nm) led to its fluorescence reemission at 490 nm. The BG concentration can be visually checked based on the fluorescence intensity on the sensor, making glucose level self-diagnosis possible.[109]

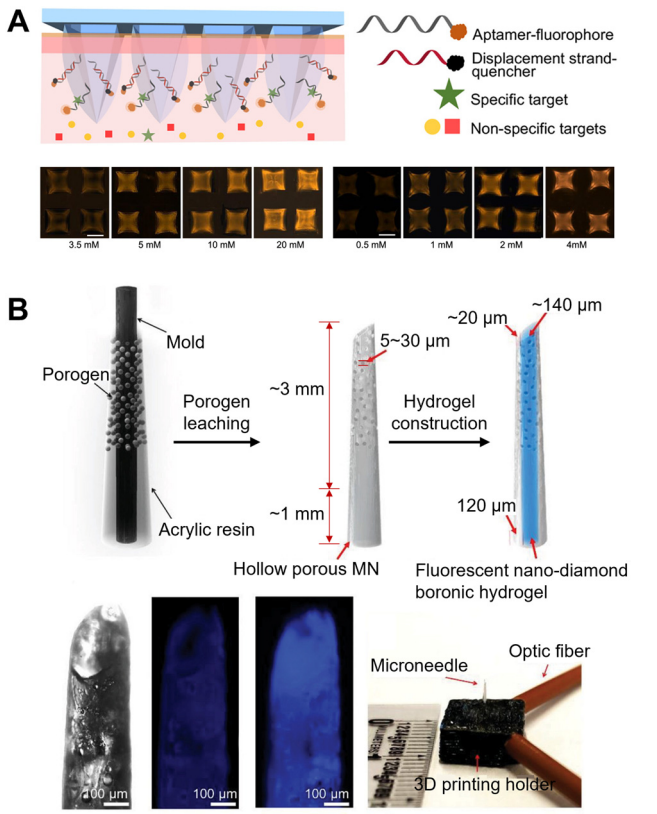

Fig. 8 MN arrays using fluorescence methods for transdermal glucose monitoring. (A) Schematic of a hydrogel MN-assisted assay integrating aptamer probes and fluorescence detection. The bottom panel represents the fluorescence images of MNs after capturing varying concentrations of ATP and glucose, respectively. Adapted with permission from ref. 104. Copyright 2022, American Chemical Society. (B) Fluorescent nanodiamond-based boronic hydrogel MNs that can detect glucose *in vitro*. The bottom panel shows the hydrogel exhibits significant fluorescence emission *in vitro*. Adapted with permission from ref. 108. Copyright 2023, Wiley-VCH.

The above examples demonstrate that the fluorescence-based MN detection platforms exhibited improved sampling efficiency, and a simplified analysis procedure. However, it is difficult to achieve an accurate quantitative detection of biomarkers in ISF, because the fluorescence signal is greatly affected by light intensity, probe stability, the penetration depth of the MNs, and human tissue variations. In addition, intricate operations and the requirement for expensive optical instruments are becoming the critical barriers for the future translation of this technique. In the future, with the assistance of miniaturized optical systems and smartphone-based portable equipment, the continuous visual detection of specific target biomarkers using MN-based fluorescent sensing devices will exhibit significant promise as a wearable platform.

4. Electrochemical MN glucose sensing

In the above sections, we introduced MNs for minimally invasive sampling and subsequent analysis by different sensing principles, including surface-enhanced Raman scattering (SERS), the colorimetric methods and fluorescence methods. Moreover, MNs were widely integrated with electrochemical glucose sensors for glucose monitoring in diabetes. Herein, we briefly introduce different mechanisms of electrochemical glucose sensing, and then illustrate their integration with MNs for minimally invasive glucose monitoring.

Generally, the core principles of electrochemical glucose sensors are converting the glucose levels into electronic signals through a chemical reaction of glucose on the electrodes.[9,110] Electrochemical glucose sensors can be broadly classified into two types, namely (i) enzymatic glucose sensors,[111] and (ii) non-enzymatic glucose sensors.[112,113] Moreover, modifying the MNs themselves with electrochemical

sensors has been widely developed for glucose monitoring. Various materials have been employed to modify the MNs, enabling them to function as either enzymatic or non-enzymatic MN glucose sensors. Below we will discuss enzymatic MN glucose sensors and non-enzymatic MN glucose sensors in detail (Table 3).

4.1. Enzymatic MN glucose sensors

4.1.1. Enzymatic glucose sensors. According to the different mechanisms of charge transfer, three generations of enzymatic glucose sensor have been proposed (Fig. 9).[9,114] The first generation of enzymatic glucose sensors immobilized the enzyme (such as GOx) on the electrode surfaces, upon which oxygen was used as oxidation mediator,[115] and the consumption of oxygen or the generation of peroxide was measured during the enzymatic reaction (Fig. 9, eqn (1)). Therefore, the glucose concentration was related to the amperometric signals from either the consumption of O_2 or the electrochemical oxidation of H_2O_2 (eqn (2) and (3)).

$$O_2 + 4H^+ + 4e^- \rightarrow 2H_2O \quad (2)$$

$$H_2O_2 \rightarrow O_2 + 2H^+ + 2e^- \quad (3)$$

This is the most commonly used mechanism for electrochemical glucose sensing. However, the first generation of enzymatic glucose sensors were limited by electroactive interference and oxygen dependence.[114] The problem of electroactive interference was usually solved by using selectively permeable membranes, which were typically composed of materials such as poly(1,3-diaminobenzene), 1,2-diaminobenzene, polypyrrole (PPy), poly(*o*-phenylenediamine), Nafion, and so on.[9,111] Meanwhile, materials such as metalized carbon,[9] Prussian blue (PB),[116] carbon nanotubes (CNTs),[117] and platinum nanoparticles (Pt NPs)[118] were employed to minimize the interference by the preferential electrocatalytic detection of

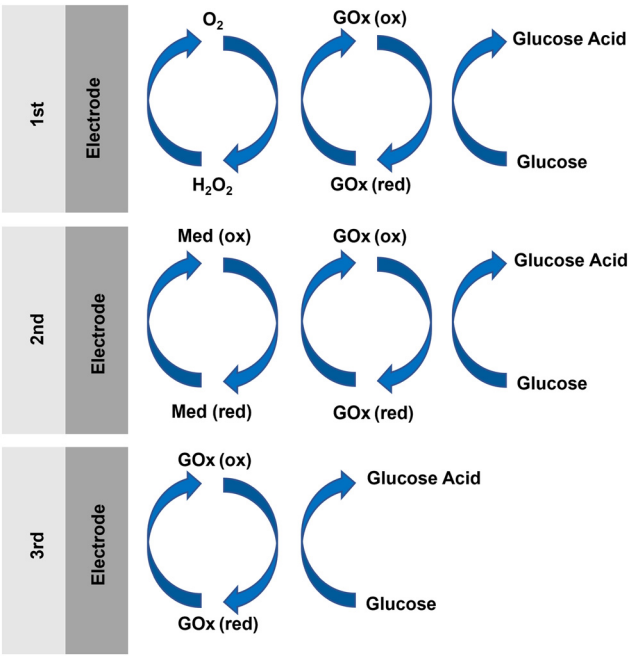

Fig. 9 Schematic illustration of redox mechanisms for the three generations of enzymatic glucose sensor.

Table 3 Comparison of different MN-based electrochemical glucose sensors

Microneedle configuration	Sensing mechanism	Application	Analytical performance	Stability	Ref.
GOx-PP, SMN	Enzymatic (1st generation)	*In vivo*	LR: 0–30 mM	3–6 h	129
GOx-PPD/SMN, HMN	Enzymatic (1st generation)	*In vitro*	LR: 0–14 mM, LOD: 0.1 mM	N.R.	130
PVC/PEGDA/GOx-CS/PPD/Pt, SMN	Enzymatic (1st generation)	*In vivo*	LR: 0–40 mM, LOD: 0.32 mM	12 h	27
Nafion/pTCA-GOx/Au/COC-PPy, SMN	Enzymatic (1st generation)	*In vivo*	LR: 0.05–20 mM	72 h	143
Nafion/GOx-BSA/OPPy-Au NPs/Au/PLA, SMN	Enzymatic (1st generation)	*In vivo*	LR: 0–2.6 mM, LOD: 40 μM	14 days	132
PVDF-Nafion/GOx-PANI/Pt NPs/Au NPs, SMN	Enzymatic (1st generation)	*In vivo*	LR: 0–20 mM, LOD: 0.1 mM	7 days	131
GOx/Pt NPs/PANI/Ti/Au, SMN	Enzymatic (1st generation)	*In vitro*	LR: 2–12 mM, LOD: 260 μM	4 days	133
GOx/PB/Au, SMN	Enzymatic (1st generation)	*In vivo*	LR: 2–12 mM, LOD: 8.65 μM	N.R.	134
PVC/CS/GOx/PB, HMN	Enzymatic (1st generation)	*In vitro*	LR: 1–10 mM	N.R.	135
Nafion/TTF/GOx, SMN	Enzymatic (2nd generation)	*In vitro*	LR: 2–20 mM	N.R.	136
TTF/GOx/CP, HMN	Enzymatic (2nd generation)	*In vitro*	LR: 5–25 mM, LOD: 0.1 mM	60 h	137
PEGDA-VF-Darocur-GOx, SMN	Enzymatic (2nd generation)	*In vitro*	LR: 0–4 mM, LOD: 1 μM	N.R.	138
MAP-GOx/FCA, SMN	Enzymatic (2nd generation)	*In vivo*	LR: 5.5–22 mM	7 days	139
GOx/Fc-PAMAM/Si/Au, SMN	Enzymatic (2nd generation)	*In vivo*	LR: 1–9 mM, LOD: 0.66 mM	N.R.	140
FADGDH/FcSH/H-PG, SMN	Enzymatic (2nd generation)	*In vitro*	LR: 0.1–10 mM, LOD: 50 μM	20 days	141
FADGDH/MB/MWCNT/Au, SMN	Enzymatic (2nd generation)	*In vitro*	LR: 0.05–5 mM, LOD: 7 μM	12 days	142
PEDOT/Pt, SMN	Enzymatic (2nd generation)	*In vitro*	LR: 2–24 mM	7 days	144
Pt NPs/MWCNTs/iron catalyst, SMN	Non-enzymatic	*In vitro*	LR: 3–20 mM	N.R.	164
Nafion/Pt black/parylene/Au, SMN	Non-enzymatic	*In vivo*	LR: 0–36 mM, LOD: 50 μM	4 days	165
Nafion/Pt black/parylene/Au, SMN	Non-enzymatic	*In vivo*	LR: 1–20 mM, LOD: 10 μM	7 days	167

Abbreviation: LR: linear range; LOD: limit of detection; N.R.: not reported; SMN: solid microneedle; HMN: hollow microneedle; GOx: glucose oxidase; FADGDH: (FAD)-dependent glucose dehydrogenase; PPD: poly(*o*-phenylenediamine); PANI: polyaniline; PP: polyphenol; Pt NPs: platinum nanoparticles; TCA: terthiophene carboxylic acid; COC: cyclic olefin copolymer; PPy: polypyrrole; BSA: bovine serum albumin; OPPy: overoxidized polypyrrole; Au NPs : gold nanoparticles; PLA: poly(lactic acid); PB: Prussian blue; PVC: polyvinyl chloride; CS: chitosan; PEGDE: poly(ethylene glycol)diglycidyl ether; TTF: tetrathiofuvalene; PEDOT: poly(3,4-ethylenedioxythiophene); CP: carbon paste; PEGDA: poly(ethylene glycol)diacrylate; VF: vinylferrocene; MB: methylene blue; MWCNT: multi-walled carbon nanotubes; FcSH: 6-(ferrocenyl)hexanethiol; MAP: mussel adhesive protein; FCA: ferrocene carboxylic acid; Fc-PAMAM: ferrocene-cored poly(amidoamine).

H_2O_2. In parallel, researchers also devoted work to conquering the limitation of oxygen dependence. For example, oxygen-rich carbon paste (CP) enzyme electrodes were developed to provide an internal supply of oxygen.[119]

Instead of using oxygen as a redox mediator, as in the first generation, the second generation of enzymatic glucose sensors employed artificial redox mediators to transport electrons from the enzyme active sites to the electrodes (Fig. 9).[120] The artificial redox mediators can accelerate the shuttling of electrons between the active sites of the enzymes and the electrode surface, therefore increasing the rate of enzymatic reaction. For instance, conductive organic salts, ferrocene and its derivatives, and ferricyanide[9,111] were commonly used as artificial redox mediators for GOx. In this generation of enzymatic glucose sensors, the catalytic reaction involves three main steps: (i) the reduction of GOx-bound flavin adenine dinucleotide (FAD) (GOx(FAD)) to form FAD-dependent glucose dehydrogenase (FADGDH), facilitated by the transfer of electrons from the glucose to the FAD reaction centers of GOx(FAD); (ii) the transfer of electrons from the FADGDH centers to an artificial mediator, resulting in the reduction of Med (ox) to Med (red); and (iii) the transportation of electrons through the artificial mediator to the electrodes.[121]

This electron transfer leads to the generation of a current signal, which can be used for glucose measurement. The efficient interaction between the enzymes and the mediators is crucial to ensure the effective transport of electrons between the redox active centers and the electrodes.[120] Various strategies have been proposed to optimize the mediators in electrode-supported enzyme films, including the use of osmium (Os) complexes as mediators, the functionalization of multi-walled carbon nanotubes (MWCNTs), GOx and binding proteins, and stabilizing artificial mediators.[122,123]

Comparably, the third generation of enzymatic glucose sensors relied on direct electron transfer (DET) between the redox center of the enzymes and the surface of the electrodes (Fig. 9).[124] Heller and coworkers first proposed the fundamental concept of DET.[125] They established a covalent connection between the active site of an enzyme and the electrode surface using a redox polymer. Besides, numerous approaches have been investigated to address the challenge of long electron tunneling distances and facilitate the direct electrochemistry of enzymes. For example, Jose *et al.* directly immobilized GOx onto the surface of an electrode composed of Au-coated MWCNTs,[126] in order to enhance the direct electrochemistry of GOx. In addition, Tasviri *et al.* developed amine-functionalized TiO_2 coated carbon nanotubes for the adsorption of GOx, and the resulting GOx-containing matrix was then utilized to modify the surface of a glass carbon electrode, facilitating direct enzyme electrochemistry.[127]

MNs integrated with enzymatic glucose sensors were mainly based on the mechanism of the first and the second generations, and we will illustrate their applications in detail.

4.1.2. MNs with oxygen as redox mediators. A considerable number of MN-based enzymatic glucose sensors were developed based on the first generation of enzymatic glucose sensors using oxygen as the redox mediator (Fig. 9).[128] In these applications, selectively permeable membranes were used to prevent electroactive interference, including electropolymerized films, particularly polyphenol (PP),[129] poly(*o*-phenylenediamine) (PPD), and PPy. These membranes confined GOx on the surface of the electrodes and improved the selectivity of the sensors.

For example, Sharma *et al.* described a CGM sensor based on an MN array electrode.[129] The device consisted of four 4 × 4 MN arrays by the casting of an epoxy-negative photoresist, where three arrays were metallized with Pt and served as the working electrode (WE), and the fourth array was metallized with Ag/AgCl and served as the reference electrode (RE). The GOx was immobilized into an electropolymerised PP film, enabling the functionalization of the electrodes in the MN array. The sensor had a linear response to glucose concentrations ranging from 0–30 mM with a response time within 15 s, and the *in vivo* evaluation was in excellent correlation with the measurements of a conventional glucose meter. Moreover, Joseph Wang and coworkers described a minimally invasive MN biosensor for glutamate and glucose monitoring.[130] Hollow MNs and solid MNs were firstly prepared by a light-curing method. The hollow MNs were capped onto the Pt-coated solid MNs to form a bi-component MN array electrode. Glutamate oxidase (GluOx) and GOx were confined to the surface of the solid MN by a PPD film. Chronoamperometry analysis showed the device to have great selectivity for glucose, and a highly sensitive and linear responsiveness in the physiological range of glucose (0–14 mM).[130] Recently, the same group reported a fully integrated wearable MN array equipped with sensors for the real-time monitoring of multiple biomarkers in tissues, including lactic acid, alcohol, and glucose (Fig. 10A).[27] The MNs were fabricated using PMMA. The WE and the counterelectrode (CE) were formed by sputtering Cr/Pt/Ag onto the MNs, while a portion of the MNs were chlorinated to produce Ag/AgCl as the RE. The innermost layer of the MN sensor was coated with PPD, and the relevant enzymes were incorporated into CS and crosslinked using poly(ethylene glycol)diglycidyl ether (PEGDE). Finally, a polyvinyl chloride (PVC) film was coated on the outer surface to limit diffusion and reduce surface contamination. The obtained MN sensor exhibited outstanding capability for the detection of three target analytes even with temporal changes. *In vivo* testing on human participants indicated that the MN biosensor provided continuous, quantitative, and real-time monitoring data, and therefore had significant clinical applicability. In addition, Chen *et al.* reported an MN sensor using polyvinylidene fluoride (PVDF)–Nafion nanomembranes as selectively permeable membranes for CGM *in vivo* (Fig. 10B).[131] On the surface of a stainless steel MN, Au and Pt NPs were decorated to improve the conductivity between the enzyme layer and the electrode, and polyaniline (PANI) nanofibers decorated with Pt worked as a supporting structure by trapping GOx.[131] The glucose sensor had a linear sensing range of 0–20 mM and a response time less than 30 s *in vitro*, and maintained a high stability for 7 days in mice. Recently, Guo's group reported a PLA-based MN

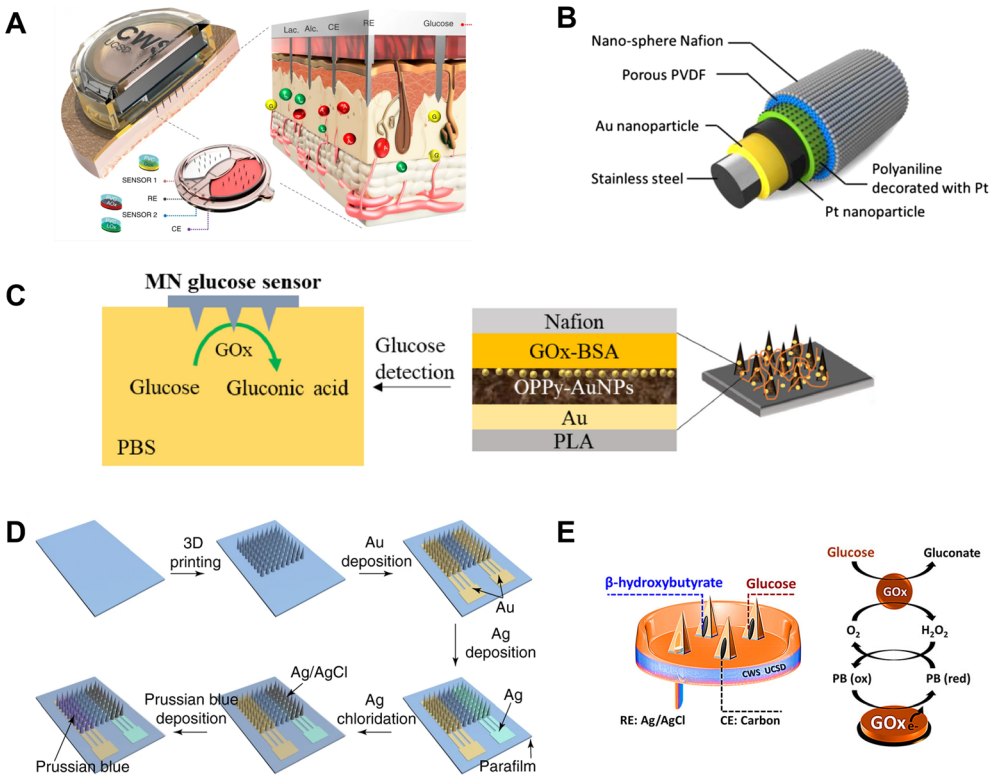

Fig. 10 Enzymatic MN glucose sensors using oxygen as a redox mediator. (A) Configuration of MN electrodes used in a multiplexed sensor component. Adapted with permission from ref. 27. Copyright 2022, Springer Nature. (B) Layered structures of MN glucose sensing. Adapted with permission from ref. 131. Copyright 2015, Elsevier. (C) Layer-by-layer structure and glucose detection scheme of an MN glucose sensor. Adapted with permission from ref. 132. Copyright 2020, Elsevier. (D) Preparation process of an integrated MN glucose sensor. Adapted with permission from ref. 134. Copyright 2021, Springer Nature. (E) Schematic illustration of dual-biomarker sensing on an MN platform. Adapted with permission from ref. 135. Copyright 2020, American Chemical Society.

glucose sensor (Fig. 10C).[132] PLA MNs were sputter-coated with a conductive layer of Au, followed by the deposition of overoxidized polypyrrole (OPPy) and Au NPs. The MNs were then functionalized with GOx-bovine serum albumin (BSA), and coated with a layer of Nafion as a permeselective membrane. The MN glucose sensor showed a good linear response in the range of 0–2.6 mM, with a sensitivity of 8.09 μA mM^{-1} and a limit of detection of 40 μM *in vitro*, and showed a high stability of 2 weeks *in vivo*.

Meanwhile, Jiang's group developed a flexible MN electrode array-based biosensor (MEAB) and a multichannel portable electrochemical analyzer (MPEA) for the concurrent detection of glucose and other target analytes.[133] The MN electrode array (MEA) was manufactured on a flexible substrate. The WE was formed by sputter coating an Au/Ti film on the MEA, and the subsequent electrodeposition of PANI nanofibers and Pt NPs. GOx and other enzymes were immobilized onto the MEA to complete the formation of the MEAB. The biosensor showed an excellent sensing performance of glucose and other blood metabolites.

Apart from Au and Pt NPs, PB can also reduce the operating potential, while its high catalytic activity enhanced the stability and selectivity of the sensor. For example, Cui *et al.* recently demonstrated the efficacy of an integrated MN biosensor for CGM in normal and diabetic mice (Fig. 10D).[134] The sensor showed a dual electrode configuration, in which the MNs coated with Au served as the WE, and Ag/AgCl-coated MNs were used for the RE/CE. A PB layer was deposited onto the WE to broaden the linear detection range of the device. GOx was immobilized on the WE to fully realize the glucose-sensing ability. The sensor showed a linear range of detection of glucose between 0.8–24 mM, with a limit of detection of 8.65 μM. Furthermore, the sensor was able to continuously monitor the subcutaneous glucose levels accurately upon implantation into the dermis of mice. Meanwhile, Joseph Wang's group developed an MN-based device for continuous ketone body monitoring (CKM), along with the detection of glucose and lactate (Fig. 10E).[135] A 2 × 2 hollow MN array was prepared by micromachining. Two MNs were used as the WEs for the simultaneous bi-component detection of β-hydroxybutyrate (HB) and glucose or lactate after CP packing and functionalization. The remaining two MNs served as the CE and the RE, respectively. When the device was used to detect a single analyte, only one MN was processed as the WE. PB, GOx, CS, and PVC were sequentially modified at one WE for glucose detection. The single analyte sensor showed a

linear dynamic range of detection of glucose between 1–10 mM in artificial ISF, with a high sensitivity of 0.036 μA mM^{-1}.

4.1.3. MNs with artificial mediators as redox mediators. Compared with the first generation of enzymatic glucose sensors which used oxygen as an oxidation mediator, the second generation of glucose sensors employed artificial mediators to overcome the oxygen dependence (Fig. 9), and are also widely integrated onto MNs for glucose monitoring.

Conductive organic salts have been widely used as electronic mediators in glucose sensors. For instance, Trzebinski *et al.* presented a microfluidic platform that integrated MN-based biosensors for glucose and lactate monitoring (Fig. 11A).[136] The MN array was prepared using SU-8 resin and metallized with gold. GOx or LOx enzyme was fixed onto the metallized MN array. Then the electron transfer mediator, tetrathiofuvalene (TTF), was deposited on the MNs. The MN array was then integrated into a microfluidic chip. The sensor had a linear response range to a glucose concentration of 2–25 mM with a response time of 15 ± 9 s and remained stable for 48 h. Similarly, Joseph Wang's group developed an MN-based self-powered biofuel-cell glucose sensor.[137] First, an array of 3 × 3 hollow MNs was printed with light-curing resin. The first row of MNs was modified with Pt black and used as the cathode, and both the second and the third rows of MNs were functionalization with GOx and TTF to serve as the anode. The anode was based on the transfer of TTF shuttle electrons from the enzyme to the electrode surface, while the cathode

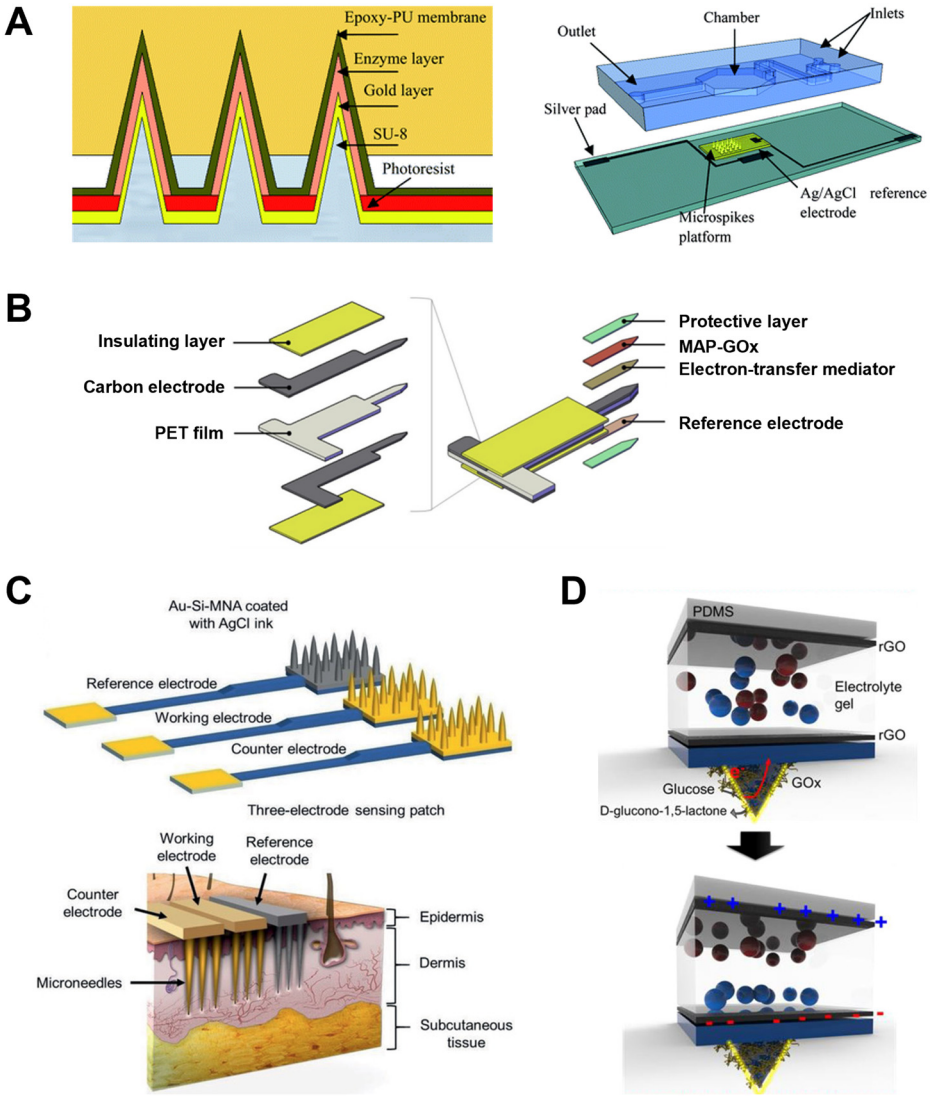

Fig. 11 Enzymatic MN glucose sensors using artificial redox mediators. (A) Preparation process of an MN-based skin patch, and the microfluidic platform integrated with the MN glucose sensor. Adapted with permission from ref. 136. Copyright 2012, The Royal Society of Chemistry. (B) Structure of an MAP-GOx/FCA/PET MN glucose sensor. Adapted with permission from ref. 139. Copyright 2019, Elsevier. (C) High-density Si MN arrays as three electrodes and their application into skin. Adapted with permission from ref. 140. Copyright 2022, Wiley-VCH. (D) Working principle of MN-based SPSCs. Adapted with permission from ref. 145. Copyright 2022, American Chemical Society.

depended on the catalytic action of Pt black for oxygen reduction. This sensor can detect different glucose concentrations from 5 to 25 mM.

Meanwhile, ferrocene and its derivatives are also commonly used as electron transport mediators in glucose sensors. Caliò *et al.* developed a multi-analyte biosensor using a polymeric MN array to monitor glucose and lactic acid levels in ISF.[138] The MN array electrode was fabricated using PEGDA doped with enzyme (GOx or LOx) and the redox mediator of vinylferrocene (VF). The VF transported the produced electrons from the redox center of the enzyme to the electrode surface. The MN-based electrode was used as the WE, and the sensors were able to measure the glucose levels in PBS, with a linear response of glucose from 0 to 4 mM, and a limit of detection of 1 μM. In addition, Cha and coworkers developed a mussel adhesive protein (MAP)-based enzymatic MN sensor for CGM (Fig. 11B).[139] A carbon layer and a Ag/AgCl layer were deposited on the front and the back of a polyethylene terephthalate (PET) film to serve as the WE and RE, respectively. The PET film was then laser-cut into a needle shape. Subsequently, the electron-transfer mediator of ferrocene carboxylic acid (FCA) was deposited onto the WE, and the MAP acted as a bioadhesive to immobilize the GOx to the WE. The obtained sensor exhibited a stable glucose response in the range of 5.5–22 mM over 7 days *in vitro*, and its effectiveness was demonstrated in diabetic beagles, cynomolgus monkeys, and human volunteers.[139] Recently, Voelcker's group reported a high-density silicon MN array patch for transdermal electrochemical glucose monitoring (Fig. 11C).[140] Two Au-coated MN arrays were used as the WE and CE, and another Au-coated MN array was further coated with AgCl as an RE. The WE was functionalized with GOx and the redox mediator of ferrocene-cored poly(amidoamine) (Fc-PAMAM) dendrimer. The MN array patch detected glucose in ISF with a linear range from 1–9 mM, and showed a strong correlation with the measurements with commercial glucose meters. In addition, Bollella reported an enzymatic sensor based on highly porous gold (H-PG) MNs for glucose monitoring in artificial ISF.[141] The sensor contained four 4 × 4 MN arrays, two of which were coated with Au and used for WEs, the third array was coated with Au and served as the CE, and the last one was coated with Ag for the RE. H-PG MNs were created by self-templating method, which involves two steps: gold electrodeposition and gas bubbling as a self-template.[141] Then the surface of H-PG MNs was coated with 6-(ferrocenyl)hexanethiol (FcSH) as a redox mediator, and immobilized with FADGDH for functionalization. Ultimately, the biosensor detected glucose in artificial ISF with a linear range of 0.1–10 mM, and a long-term stability of 20 days. Meanwhile, the same group also developed an MN biosensor array for the minimally invasive and continuous monitoring of both glucose and lactic acid levels in artificial ISF.[142] MWCNTs were electrodeposited on the surface of WEs, and methylene blue (MB) was deposited as the redox mediator. The FADGDHs and LOx were fixed onto two WEs through drop-casting, respectively. Both the lactate and glucose sensors had an excellent performance in artificial ISF, where the glucose sensor showed a good linear range of 0.05–5 mM with a detection limit of 7 μM.

Enzymes can also be bonded to the surface of the polymer MNs, allowing a direct transfer of electrons from the enzyme redox site to the electrode through the polymer network. For example, Kim *et al.* developed a minimally invasive wireless biosensor for CGM.[143] First, an MN array composed of a cyclic olefin copolymer and PPy was coated with gold to form AuMN. GOx was covalently bound with terthiophene carboxylic acid (TCA) and then electropolymerized on AuMNs to form the WE. The sensor exhibited a good linear response in the range of 0.05–20 mM glucose. By coupling the sensor to a wireless transmitter, the measurements could be transmitted to a mobile phone *via* bluetooth, and the data were consistent with the measurement by fingertip sampling.

Moreover, the slight swelling of conductive polymers such as poly(3,4-ethylenedioxythiophene) (PEDOT) in aqueous media prevents the escape of enzyme, and therefore can serve as both an electronic mediator for sensing and an immobilization agent for the enzyme. For example, Anderson's group developed a conducting polymer-based MN patch for CGM.[144] The stainless steel MNs were coated with Pt, and then PEDOT was coated as an electrical mediator and immobilization agent for GOx. The slight swelling of the PEDOT enhanced glucose diffusing into the enzymes for signal transduction. The sensor exhibited linearity over a range of 2–24 mM glucose and could remain relatively stable for 7 days.

Besides the commonly used enzymatic sensing mechanism, MNs based on self-powered solid-state supercapacitors (SPSCs) were recently developed for CGM (Fig. 11D).[145] Herein, both a PDMS thin film and the substrate of PDMS MN platform were coated with graphene oxide and electrolyte gel. The MN array was further coated with an enzyme layer (GOx) and an electrode layer of PEDOT:PSS. The assembly of the two surfaces formed the SPSC (Fig. 11D). The GOx on the surface of the MNs encountered the glucose in ISF, and electrons created by glucose oxidation resulted in self-charging of the supercapacitor. This capacitor can distinguish normal, pre-diabetic and diabetic artificial skins *in vitro*.

4.2. Non-enzymatic MN glucose sensors

4.2.1. Non-enzymatic glucose sensors. As above described, enzymatic glucose sensors possess great selectivity and sensitivity in detecting analytes; however, enzyme immobilization was relatively complex and their stability was limited, which led to deactivation of the enzyme. Moreover, the results of the enzymatic sensors were greatly influenced by external factors such as temperature, humidity, and pH.[112,113] Compared with enzymatic sensors, non-enzymatic sensors show advantages such as good stability and reproducibility, and are free from oxygen limitation.[146,147] Extensive studies have been explored for non-enzymatic glucose sensors, generally through the direct electrochemical oxidation of nanomaterials, such as metals (Pt, Au, Ni, Cu, *etc.*), metal–oxides (NiO, CuO, *etc.*), metal sulfides, metal–organic frameworks (MOFs), metal–

azolate frameworks (MAFs), carbon materials, and so on.[113,148,149]

Most metals have great electrical conductivity. To date, precious metals including Au and Pt and transition metals including Co and Ni have been extensively used in the design of non-enzymatic glucose sensors.[113,147] Large bulks of Pt and Au were the earliest electrode materials used in non-enzymatic electrochemical sensors.[147] However, Pt and Au electrodes showed several shortcomings in the electrocatalytic oxidation of glucose, including the adsorption of intermediate products, lack of selectivity of analytes, influence of ions, and so on.[147] To address these drawbacks, nanoscale precious metal materials were prepared to enhance the specific surface area and roughness, to mitigate the aforementioned challenges.[150] In addition, alloy forms of precious metals are frequently used for the development of non-enzymatic sensors.[151,152] These alloys encompass various compositions, including precious–precious metal combinations, precious metals combined with other metals, and bimetallic and trimetallic alloys, *et al.*

Apart from precious metals, transition metals such as Ni and Cu, along with their corresponding compounds, are extensively employed in the fabrication of non-enzymatic glucose sensors. In comparison with precious metals, transition metals offer the advantage of being abundant in nature and more cost-effective.[153] Previous study demonstrated the catalytic potential of Ni NPs in organic reactions, including the direct oxidation of glucose in alkaline environments.[154] Moreover, various nickel-based materials, such as NiO, Ni$(OH)_2$, Ni_3N, Ni_2P, $Ni_3(PO_4)_2$, Ni-MOF, and Ni alloys, are widely employed in glucose catalysis.[155] The electrooxidation of glucose took place on the surface of the nickel-based materials, involving electron transfer between the Ni^{3+}/Ni^{2+} redox couple, regardless of the initial form of the nickel-based material.[156] In parallel, Cu-based materials can facilitate the electrical catalysis of glucose.[147] Metallic copper, CuO, Cu_2O, $Cu(OH)_2$, Cu_3N, CuS, and Cu_3P participate in the reaction in various morphological structures, including nanorods, nanowires, nanoflowers, nanoflakes, and nanocubes. Given their high aspect ratio, metallic copper is frequently employed in the form of nanowires in electrochemical glucose sensors.[157,158] The catalytic mechanism of copper-based materials is mediated by the Cu^{3+}/Cu^{2+} redox couple under alkaline conditions.[112] In addition, other metals, such as Co, Zn, Fe, Mo, Ag, Mn, *etc*. play an important role in the design of non-enzymatic glucose sensors.[159–161] Moreover, carbon-based materials, including carbon dots, carbon nanotubes, carbon fibers, graphene, and fullerenes, have attracted great attention as catalytic materials for electrochemical sensors, due to their unique physical and chemical properties.[162,163]

4.2.2. MNs with non-enzymatic glucose sensors. The above section highlights the mechanism of non-enzymatic glucose sensors relying on diverse materials. Herein, we focus on the detailed applications of MN-based non-enzymatic glucose sensors.

Yoon *et al.* developed a three-electrode integrated electrochemical sensor using MNs (Fig. 12A).[164] Iron catalyst was deposited on a part of a silicon MN array, which resulted in the formation of the WE and CE. Subsequently, MWCNTs were grown and Pt NPs were deposited on the iron catalyst-coated MN array. Ag was deposited and chlorinated onto another part of the MNs to form the RE. The sensor demonstrated a linear amperometric response to a glucose concentration in the range of 3–20 mM, with a sensitivity of 17.73 ± 3 μA mM^{-1} cm^{-2}, which surpassed the sensitivity of numerous enzymatic sensors.[140,143]

In addition, Lee *et al.* proposed an MN-based non-enzymatic biosensor for painless CGM (Fig. 12B).[165] The substrate of a stainless steel MN array was electroplated with a layer of gold, followed by passivation with a parylene coating. Then a Pt black layer was coated on the tip of each MN. The obtained MN array was employed as the WE, and Ag/AgCl was electroplated onto another MN array as the RE/CE. The sensitivity of the sensor reached 1.62 μA mM^{-1}, it can detect glucose in a range of 0–32 mM with a response time of 13 s, and the sensor was able to function for 4 days upon attachment onto rabbit skin.

Similarly, Cho's group proposed an MN-based amperometric non-enzymatic glucose sensor for CGM (Fig. 12C).[166] The preparation and treatment of the MNs were similar to the above work.[165] In the three-electrode configuration, the MN electrode was employed as the WE, while a Pt coil served as the CE, and Ag/AgCl was utilized as the RE. In the double-electrode configuration, the Ag/AgCl MN was utilized as the CE. The sensor with three electrodes had a linear response within a larger range (1–40 mM), whereas the sensor with two MN electrodes exhibited a greater sensitivity (205.57 ± 48.65 μA mM^{-1} cm^{-2}), and a lower detection limit (6.0 ± 1.0 μM). More recently, the same group optimized the MN electrode by porous Pt black, and the sensor exhibited a lifespan of 7 days when applied into the skin of rats.[167]

4.3. Other MN-integrated electrochemical glucose sensors

In the above sections, MNs themselves were modified to serve as electrodes for electrochemical glucose sensing. However, in other cases, MNs were only used for the sampling or extraction of ISF as described in section 2, and then electrochemical sensing mechanisms were integrated with the MN system for glucose monitoring.[43,45,168] Herein, we briefly describe the applications of these types of MN integrated with electrochemical glucose-sensing mechanisms.

Jina *et al.* reported an MN-based CGM device, which used a hollow silicon MN array to extract ISF, and the electrochemical glucose sensor was placed on the back of the MN array.[168] Strambini *et al.* proposed an MN-based self-powered biosensor for the painless, high-precision measurement of glucose in ISF.[43] Hollow silica MNs were used to efficiently collect ISF by capillary action, and were coupled with external electrode sensors on the back of the MN patch. The sensors showed an excellent sensing performance of glucose in synthetic ISF.[43] Ribet *et al.* proposed a CGM device consisting of a single hollow MN and a sensing probe assembled inside the lumen

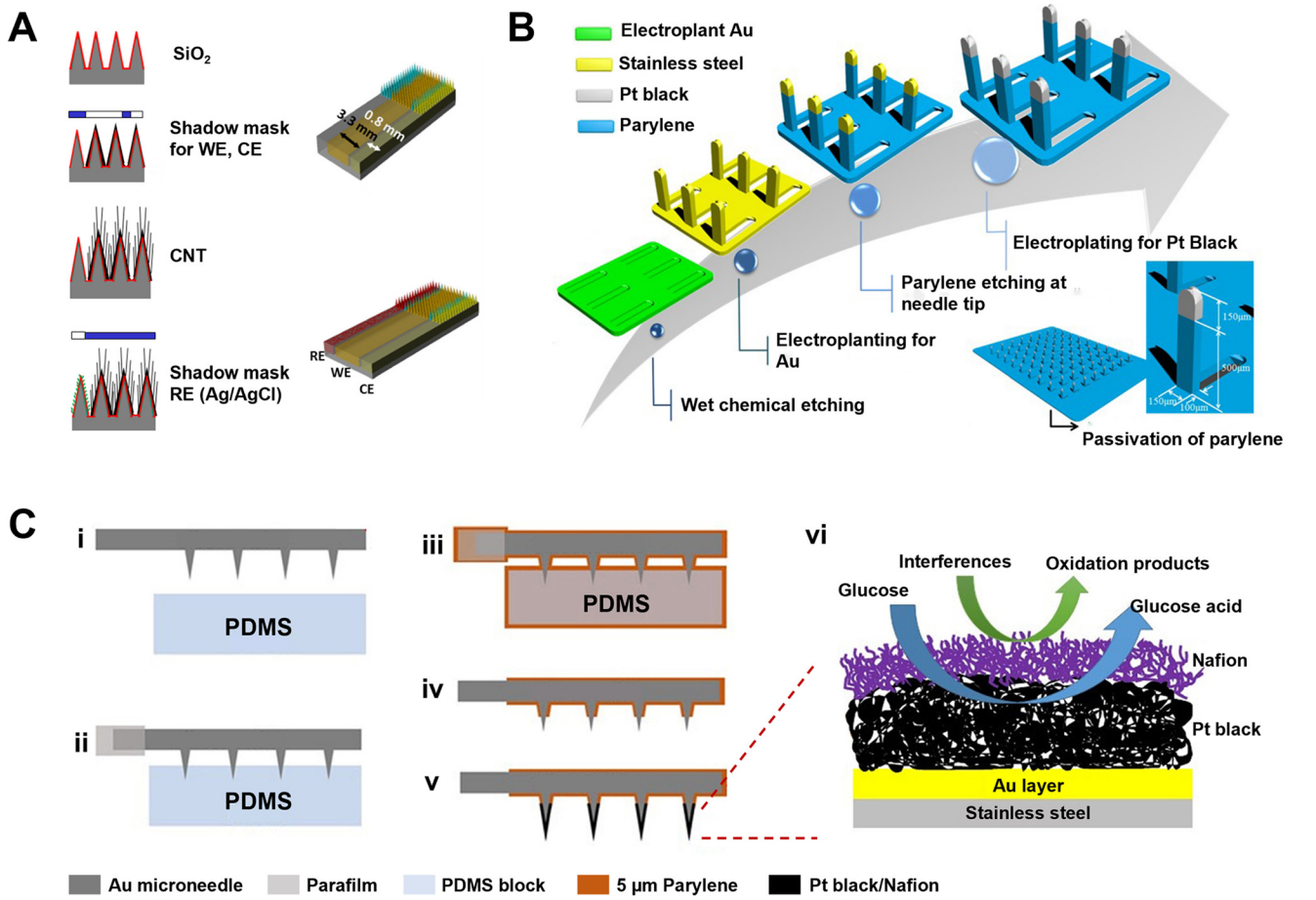

Fig. 12 Non-enzymatic MN glucose sensors. (A) Preparation of a three-electrode MN-based non-enzymatic glucose sensor. Adapted with permission from ref. 164. Copyright 2013, MDPI. (B) Fabrication of a 3D MN array with Pt black catalytic layer for a non-enzymatic glucose sensor. Adapted with permission from ref. 165. Copyright 2016, Elsevier. (C) Non-enzymatic detection of glucose based on a Pt black coated MN array. (i–v) Preparation process of a Nafion/Pt black/parylene/AuMN electrode. (vi) Working mechanism of the MN glucose sensor. Adapted with permission from ref. 166. Copyright 2018, Springer Nature.

of the MN. The system provided minimally invasive, rapid, and trustworthy CGM for patients with diabetes.[45]

In addition, the iontophoresis mentioned in section 2.4 was also an effective method for sampling that can be integrated with electrochemical glucose sensors.[21,74,75] Furthermore, Xie's group developed an integrated MN theranostic platform (MNTP) inspired by the animal masticatory system (Fig. 13A).[169] The MN array penetrated into the skin layer using a circuit-connected pressing belt allowing for the exudation of ISF, and the subsequent detection of glucose and other biomarkers was carried out by a planar multielectrode array located underneath the MN array. The sensing results were then transmitted to a drug delivery device, thereby enabling the realization of a closed-loop system. Besides, Zheng *et al.* prepared a wire electrode-embedded MN patch for glucose detection in skin ISF or plant ISF (Fig. 13B).[170] The MNs were prepared by a silk fibroin solution, and the electrode wires were embedded in the MNs before solidification. The sensor exhibited a sensitive linear response in the range of 3–18 mM glucose in the skin ISF and 30–180 mM in the plant ISF.

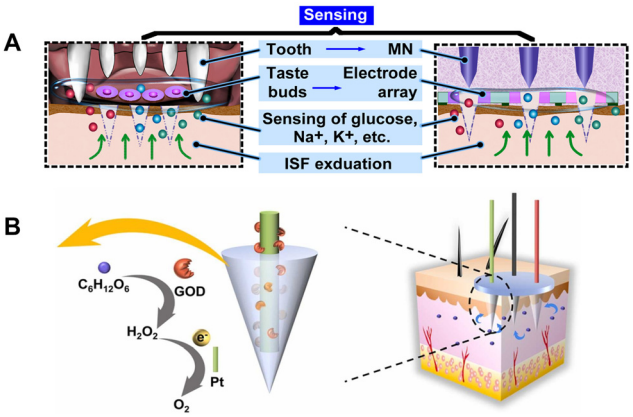

Fig. 13 Integration of MNs for sampling and glucose sensing. (A) Illustration of transdermal sensing of an MN theranostic platform. Adapted with permission from ref. 169. Copyright 2022, American Association for the Advancement of Science. (B) Working mechanism of wire electrode-embedded MN patches. Adapted with permission from ref. 170. Copyright 2022, Elsevier.

5. Conclusion and perspectives

In this review, we summarize MN-based glucose detection and sensing devices in detail. MNs served as a sampling tool to facilitate the extraction of ISF and blood by means of an external negative pressure, capillary force, swelling force, or iontophoresis, which play an important role in ISF detection coupled with *in vitro* diagnostic systems.

Raman methods, colorimetry, fluorescence, and electrochemical sensing mechanisms have been integrated with MN systems to enhance the development of MN sensors. Compared with traditional BG monitoring, MNs have the advantages of a minimally invasive, painless, rapid readout, and miniaturization, and thus the integration of these detection technologies enables the MN system's sampling, sensing and monitoring functions, making this a promising platform for biomedical applications. MN glucose sensors are important parts of wearable technologies, owing to their self-powering capability, non-invasive nature, and there is no need to integrate a signal transmission system.

In recent years, electrochemical MN glucose sensors have been the dominant type of wearable glucose sensor. With the integration of electrochemical systems and wireless communication technologies, the collected data can be transferred to a platform for analysis and application, enabling data visualization. Numerous studies have met the need for intelligent, miniaturized, wearable glucose sensors. As a result, electrochemical MN glucose sensors hold significant promise for use in CGM systems.

In future research, the development of the sensors will focus on the enzyme stability of enzymatic glucose-sensing systems and the biofouling problems of sensing systems. Optimizing the power supply and addressing the need for real-time calibration, detection, and analysis will be crucial to advancing the field of CGM. Additionally, the combined detection of multiple analytes is necessary to obtain comprehensive disease-related biomarker information. Designing the layout of the MNs and integrating compound types of sensor can realize all-in-one MN-based biosensors for the simultaneous and multiplexed detection of analytes.

With further technique crossovers and numerous reliable clinical trials, MN-based devices could pave the way for personalized diabetes care and self-health management for millions of people worldwide.

Abbreviations

1-DT	1-Decanethiol
Au NPs	Gold nanoparticles
Au NRs	Gold nanorods
BG	Blood glucose
BSA	Bovine serum albumin
CE	Counterelectrode
CGM	Continuous glucose monitoring
CKM	Continuous ketone body monitoring
CNT	Carbon nanotube
CP	Carbon paste
CS	Chitosan
DET	Direct electron transfer
DM	Diabetes mellitus
DRIE	Deep-reactive ion etching
EOF	Electroosmotic flow
FADGDH	FAD-dependent glucose dehydrogenase
FCA	Ferrocene carboxylic acid
Fc-PAMAM	Ferrocene-cored poly(amidoamine)
FcSH	6-(Ferrocenyl)hexanethiol
FDA	Food and Drug Administration
FPBA	Fluorophenylboronic acid
GelMA	Gelatin methacryloyl
GluOx	Glutamate oxidase
GOx	Glucose oxidase
H_2O_2	Hydrogen peroxide
HB	Hydroxybutyrateand
H-PG	Highly porous gold
HRP	Horseradish peroxidase
IDF	International Diabetes Federation
ISF	Interstitial fluid
LOx	Lactate oxidase
MAF	Metal–azolate frame work
MAP	Mussel adhesive protein
MB	Methylene blue
MEA	Microneedle electrode array
MEAB	Microneedle electrode array-based biosensor
MeHA	Methacrylated hyaluronic acid
MN	Microneedle
MOF	Metal–organic framework
MPEA	Multichannel portable electrochemical analyzer
MWCNTs	Multi-walled carbon nanotubes
OPPy	Overoxidized polypyrrole
PANI	Polyaniline
PB	Prussian blue
PBA	Phenylboronic acid
PDA	Polydopamine
PDMS	Polydimethylsiloxane
PEDOT	Poly(3,4-ethylenedioxythiophene)
PEG	Poly(ethylene glycol)
PEGDA	Poly(ethylene glycol)diacrylate
PEGDE	Poly(ethylene glycol)diglycidyl ether
PET	Polyethylene terephthalate
PGMA	Poly(glycidyl methacrylate)
PLA	Poly(lactic acid)
PLGA	Poly(lactic-*co*-glycolic acid)
PMMA	Poly(methyl methacrylate)
POCT	Point-of-care testing
PP	Polyphenol
PPD	Poly(*o*-phenylenediamine)
PPy	Polypyrrole
PSS	Poly(styrenesulfonate)
Pt NPs	Platinum nanoparticles
PVA	Polyvinyl alcohol
PVC	Polyvinyl chloride

PVF	Polyvinyl formal
PVP	Polyvinylpyrrolidone
RE	Reference electrode
RI	Reverse iontophoresis
SERS	Surface-enhanced Raman scattering
SPSC	Self-powered solid-state supercapacitors
TCA	Terthiophene carboxylic acid
TMB	Tetramethylbenzidine
TOPS	*N*-Ethyl-*N*-sulfopropyl-M-toluidine
TTF	Tetrathiofuvalene
VF	Vinylferrocene
WE	Working electrode

Conflicts of interest

There are no conflicts of interest to declare.

Acknowledgements

The work was supported by the National Natural Science Foundation of China (NSFC, grant number: 82172096), Guangdong Basic and Applied Basic Research Foundation (2021A1515012183), and Science and Technology Program of Shenzhen (JCYJ20220530140610022) for financial support.

References

1 H. Sun, P. Saeedi, S. Karuranga, M. Pinkepank, K. Ogurtsova, B. B. Duncan, C. Stein, A. Basit, J. C. N. Chan, J. C. Mbanya, M. E. Pavkov, A. Ramachandaran, S. H. Wild, S. James, W. H. Herman, P. Zhang, C. Bommer, S. Kuo, E. J. Boyko and D. J. Magliano, IDF Diabetes Atlas: Global, regional and country-level diabetes prevalence estimates for 2021 and projections for 2045, *Diabetes Res. Clin. Pract.*, 2022, **183**, 109119.

2 M. A. Atkinson, G. S. Eisenbarth and A. W. Michels, Type 1 diabetes, *Lancet*, 2014, **383**, 69–82.

3 Y. Zheng, S. H. Ley and F. B. Hu, Global aetiology and epidemiology of type 2 diabetes mellitus and its complications, *Nat. Rev. Endocrinol.*, 2018, **14**, 88–98.

4 S. Haxha and J. Jhoja, Optical based noninvasive glucose monitoring sensor prototype, *IEEE Photonics J.*, 2016, **8**, 1–11.

5 M. Elsherif, M. U. Hassan, A. K. Yetisen and H. Butt, Hydrogel optical fibers for continuous glucose monitoring, *Biosens. Bioelectron.*, 2019, **137**, 25–32.

6 K. Singh, T. Agarwal, U. Kumar, S. Pal, A. Runthala, T.-M. Pan and C. C. Wu, Optical biosensors for diabetes management: Advancing into stimuli-responsive sensing mechanisms, *Smart Mater. Med.*, 2023, **4**, 91–101.

7 Y. Chen, S. Lu, S. Zhang, Y. Li, Z. Qu, Y. Chen, B. Lu, X. Wang and X. Feng, Skin-like biosensor system via electrochemical channels for noninvasive blood glucose monitoring, *Sci. Adv.*, 2017, **3**, 1701629.

8 A. J. Bandodkar, P. Gutruf, J. Choi, K. Lee, Y. Sekine, J. T. Reeder, W. J. Jeang, A. J. Aranyosi, S. P. Lee, J. B. Model, R. Ghaffari, C.-J. Su, J. P. Leshock, T. Ray, A. Verrillo, K. Thomas, V. Krishnamurthi, S. Han, J. Kim, S. Krishnan, T. Hang and J. A. Rogers, Battery-free, skin-interfaced microfluidic/electronic systems for simultaneous electrochemical, colorimetric, and volumetric analysis of sweat, *Sci. Adv.*, 2019, **5**, 3294.

9 H. Teymourian, A. Barfidokht and J. Wang, Electrochemical glucose sensors in diabetes management: an updated review (2010–2020), *Chem. Soc. Rev.*, 2020, **49**, 7671–7709.

10 C. Wang, H.-S. Zeng, K.-X. Liu, Y.-N. Lin, H. Yang, X.-Y. Xie, D.-X. Wei and J.-W. Ye, Biosensor-based therapy powered by synthetic biology, *Smart Mater. Med.*, 2023, **4**, 212–224.

11 M. Bariya, H. Y. Y. Nyein and A. Javey, Wearable sweat sensors, *Nat. Electron.*, 2018, **1**, 160–171.

12 Y. J. Lin, M. Bariya, H. Y. Y. Nyein, L. Kivimaki, S. Uusitalo, E. Jonsson, W. B. Ji, Z. Yuan, T. Happonen, C. Liedert, J. Hiltunen, Z. Y. Fan and A. Javey, Porous enzymatic membrane for nanotextured glucose sweat sensors with high stability toward reliable noninvasive health monitoring, *Adv. Funct. Mater.*, 2019, **29**, 1902521.

13 T. Arakawa, Y. Kuroki, H. Nitta, P. Chouhan, K. Toma, S. Sawada, S. Takeuchi, T. Sekita, K. Akiyoshi, S. Minakuchi and K. Mitsubayashi, Mouthguard biosensor with telemetry system for monitoring of saliva glucose: a novel cavitas sensor, *Biosens. Bioelectron.*, 2016, **84**, 106–111.

14 J. Kim, M. Kim, M. S. Lee, K. Kim, S. Ji, Y. T. Kim, J. Park, K. Na, K. H. Bae, H. K. Kim, F. Bien, C. Y. Lee and J. U. Park, Wearable smart sensor systems integrated on soft contact lenses for wireless ocular diagnostics, *Nat. Commun.*, 2017, **8**, 14997.

15 J. Park, J. Kim, S.-Y. Kim, W. H. Cheong, J. Jang, Y.-G. Park, K. Na, Y.-T. Kim, J. H. Heo, C. Y. Lee, J. H. Lee, F. Bien and J.-U. Park, Soft, smart contact lenses with integrations of wireless circuits, glucose sensors, and displays, *Sci. Adv.*, 2018, **4**, 9841.

16 P. R. Miller, R. M. Taylor, B. Q. Tran, G. Boyd, T. Glaros, V. H. Chavez, R. Krishnakumar, A. Sinha, K. Poorey, K. P. Williams, S. S. Branda, J. T. Baca and R. Polsky, Extraction and biomolecular analysis of dermal interstitial fluid collected with hollow microneedles, *Commun. Biol.*, 2018, **1**, 173.

17 P. P. Samant, M. M. Niedzwiecki, N. Raviele, V. Tran, J. Mena-Lapaix, D. I. Walker, E. I. Felner, D. P. Jones, G. W. Miller and M. R. Prausnitz, Sampling interstitial fluid from human skin using a microneedle patch, *Sci. Transl. Med.*, 2020, **12**, 285.

18 T. Siegmund, L. Heinemann, R. Kolassa and A. Thomas, Discrepancies between blood glucose and interstitial glucose-technological artifacts or physiology: Implications

for selection of the appropriate therapeutic target, *J. Diabetes Sci. Technol.*, 2017, **11**, 766–772.

19 M. M. Niedzwiecki, P. Samant, D. I. Walker, V. Tran, D. P. Jones, M. R. Prausnitz and G. W. Miller, Human suction blister fluid composition determined using high-resolution metabolomics, *Anal. Chem.*, 2018, **90**, 3786–3792.

20 L. Lipani, B. G. R. Dupont, F. Doungmene, F. Marken, R. M. Tyrrell, R. H. Guy and A. Ilie, Non-invasive, transdermal, path-selective and specific glucose monitoring via a graphene-based platform, *Nat. Nanotechnol.*, 2018, **13**, 504–511.

21 J. Kim, J. R. Sempionatto, S. Imani, M. C. Hartel, A. Barfidokht, G. Tang, A. S. Campbell, P. P. Mercier and J. Wang, Simultaneous monitoring of sweat and interstitial fluid using a single wearable biosensor platform, *Adv. Sci.*, 2018, **5**, 1800880.

22 Y. Cheng, X. Gong, J. Yang, G. Zheng, Y. Zheng, Y. Li, Y. Xu, G. Nie, X. Xie, M. Chen, C. Yi and L. Jiang, A touch-actuated glucose sensor fully integrated with microneedle array and reverse iontophoresis for diabetes monitoring, *Biosens. Bioelectron.*, 2022, **203**, 114026.

23 M. Ali, S. Namjoshi, H. A. E. Benson, Y. Mohammed and T. Kumeria, Dissolvable polymer microneedles for drug delivery and diagnostics, *J. Controlled Release*, 2022, **347**, 561–589.

24 J. Wang, Z. Lu, R. Cai, H. Zheng, J. Yu, Y. Zhang and Z. Gu, Microneedle-based transdermal detection and sensing devices, *Lab Chip*, 2023, **23**, 869–887.

25 T. M. Blicharz, P. Gong, B. M. Bunner, L. L. Chu, K. M. Leonard, J. A. Wakefield, R. E. Williams, M. Dadgar, C. A. Tagliabue, R. El Khaja, S. L. Marlin, R. Haghgooie, S. P. Davis, D. E. Chickering and H. Bernstein, Microneedle-based device for the one-step painless collection of capillary blood samples, *Nat. Biomed. Eng.*, 2018, **2**, 151–157.

26 D. Kim, Y. Cao, D. Mariappan, M. S. Bono Jr., A. J. Hart and B. Marelli, A microneedle technology for sampling and sensing bacteria in the food supply chain, *Adv. Funct. Mater.*, 2021, **31**, 2005370.

27 F. Tehrani, H. Teymourian, B. Wuerstle, J. Kavner, R. Patel, A. Furmidge, R. Aghavali, H. Hosseini-Toudeshki, C. Brown, F. Zhang, K. Mahato, Z. Li, A. Barfidokht, L. Yin, P. Warren, N. Huang, Z. Patel, P. P. Mercier and J. Wang, An integrated wearable microneedle array for the continuous monitoring of multiple biomarkers in interstitial fluid, *Nat. Biomed. Eng.*, 2022, **6**, 1214–1224.

28 R. Paul, A. C. Saville, J. C. Hansel, Y. Ye, C. Ball, A. Williams, X. Chang, G. Chen, Z. Gu, J. B. Ristaino and Q. Wei, Extraction of plant DNA by microneedle patch for rapid detection of plant diseases, *ACS Nano*, 2019, **13**, 6540–6549.

29 H. Lee, T. K. Choi, Y. B. Lee, H. R. Cho, R. Ghaffari, L. Wang, H. J. Choi, T. D. Chung, N. Lu, T. Hyeon, S. H. Choi and D. H. Kim, A graphene-based electrochemical device with thermoresponsive microneedles for diabetes monitoring and therapy, *Nat. Nanotechnol.*, 2016, **11**, 566–572.

30 J. Yu, J. Wang, Y. Zhang, G. Chen, W. Mao, Y. Ye, A. R. Kahkoska, J. B. Buse, R. Langer and Z. Gu, Glucose-responsive insulin patch for the regulation of blood glucose in mice and minipigs, *Nat. Biomed. Eng.*, 2020, **4**, 499–506.

31 X. X. Zhang, G. P. Chen, F. K. Bian, L. J. Cai and Y. J. Zhao, Encoded microneedle arrays for detection of skin interstitial fluid biomarkers, *Adv. Mater.*, 2019, **31**, 1902825.

32 Q. Yang, Y. Wang, T. Liu, C. Wu, J. Li, J. Cheng, W. Wei, F. Yang, L. Zhou, Y. Zhang, S. Yang and H. Dong, Microneedle array encapsulated with programmed DNA hydrogels for rapidly sampling and sensitively sensing of specific microRNA in dermal interstitial fluid, *ACS Nano*, 2022, **16**, 18366–18375.

33 Z. Wang, J. Luan, A. Seth, L. Liu, M. You, P. Gupta, P. Rathi, Y. Wang, S. Cao, Q. Jiang, X. Zhang, R. Gupta, Q. Zhou, J. J. Morrissey, E. L. Scheller, J. S. Rudra and S. Singamaneni, Microneedle patch for the ultrasensitive quantification of protein biomarkers in interstitial fluid, *Nat. Biomed. Eng.*, 2021, **5**, 64–76.

34 P. P. Samant and M. R. Prausnitz, Mechanisms of sampling interstitial fluid from skin using a microneedle patch, *Proc. Natl. Acad. Sci. U. S. A.*, 2018, **115**, 4583–4588.

35 P. M. Wang, M. Cornwell and M. R. Prausnitz, Minimally invasive extraction of dermal interstitial fluid for glucose monitoring using microneedles, *Diabetes Technol. Ther.*, 2005, **7**, 131–141.

36 C. G. Li, K. Lee, C. Y. Lee, M. Dangol and H. Jung, A minimally invasive blood-extraction system: Elastic self-recovery actuator integrated with an ultrahigh-aspect-ratio microneedle, *Adv. Mater.*, 2012, **24**, 4583–4586.

37 C. G. Li, H. A. Joung, H. Noh, M. B. Song, M. G. Kim and H. Jung, One-touch-activated blood multidiagnostic system using a minimally invasive hollow microneedle integrated with a paper-based sensor, *Lab Chip*, 2015, **15**, 3286–3292.

38 C. Kolluru, M. Williams, J. Chae and M. R. Prausnitz, Recruitment and collection of dermal interstitial fluid using a microneedle patch, *Adv. Healthcare Mater.*, 2019, **8**, 1801262.

39 T. Leivo, U. Kiistala, M. Vesterinen, K. Owaribe, R. E. Burgeson, I. Virtanen and A. Oikarinen, Re-epithelialization rate and protein expression in the suction-induced wound model: comparison between intact blisters, open wounds and calcipotriol-pretreated open wounds, *Br. J. Dermatol.*, 2000, **142**, 991–1002.

40 M. Zheng, Z. Wang, H. Chang, L. Wang, S. W. T. Chew, D. C. S. Lio, M. Cui, L. Liu, B. C. K. Tee and C. Xu, Osmosis-powered hydrogel microneedles for microliters of skin interstitial fluid extraction within minutes, *Adv. Healthcare Mater.*, 2020, **9**, 1901683.

41 T. Li, A. Barnett, K. L. Rogers and Y. B. Gianchandani, A blood sampling microsystem for pharmacokinetic appli-

cations: design, fabrication, and initial results, *Lab Chip*, 2009, **9**, 3495–3503.
42 E. V. Mukerjee, S. D. Collins, R. R. Isseroff and R. L. Smith, Microneedle array for transdermal biological fluid extraction and in situ analysis, *Sens. Actuators, A*, 2004, **114**, 267–275.
43 L. M. Strambini, A. Longo, S. Scarano, T. Prescimone, I. Palchetti, M. Minunni, D. Giannessi and G. Barillaro, Self-powered microneedle-based biosensors for pain-free high-accuracy measurement of glycaemia in interstitial fluid, *Biosens. Bioelectron.*, 2015, **66**, 162–168.
44 Y. Li, H. Zhang, R. Yang, Y. Laffitte, U. Schmill, W. Hu, M. Kaddoura, E. J. M. Blondeel and B. Cui, Fabrication of sharp silicon hollow microneedles by deep-reactive ion etching towards minimally invasive diagnostics, *Microsyst. Nanoeng.*, 2019, **5**, 41.
45 F. Ribet, G. Stemme and N. Roxhed, Real-time intradermal continuous glucose monitoring using a minimally invasive microneedle-based system, *Biomed. Microdevices*, 2018, **20**, 101.
46 X. Q. You, Q. Y. He, T. W. Wu, D. Y. Huang, Z. Z. Peng, D. Y. Chen, Z. Chen and J. Liu, Multi-groove microneedles based wearable colorimetric sensor for simple and facile glucose detection, *Microchem. J.*, 2023, **190**, 108570.
47 S. Gholami, M. M. Mohebi, E. Hajizadeh-Saffar, M. H. Ghanian, I. Zarkesh and H. Baharvand, Fabrication of microporous inorganic microneedles by centrifugal casting method for transdermal extraction and delivery, *Int. J. Pharm.*, 2019, **558**, 299–310.
48 G. Gao, L. Zhang, Z. Li, S. Ma and F. Ma, Porous microneedles for therapy and diagnosis: Fabrication and challenges, *ACS Biomater. Sci. Eng.*, 2023, **9**, 85–105.
49 L. Bao, J. Park, G. Bonfante and B. Kim, Recent advances in porous microneedles: materials, fabrication, and transdermal applications, *Drug Delivery Transl. Res.*, 2022, **12**, 395–414.
50 L. Liu, H. Kai, K. Nagamine, Y. Ogawa and M. Nishizawa, Porous polymer microneedles with interconnecting microchannels for rapid fluid transport, *RSC Adv.*, 2016, **6**, 48630–48635.
51 J. Chen, M. Wang, Y. Ye, Z. Yang, Z. Ruan and N. Jin, Fabrication of sponge-forming microneedle patch for rapidly sampling interstitial fluid for analysis, *Biomed. Microdevices*, 2019, **21**, 63.
52 K. Yi, Y. Wang, K. Shi, J. Chi, J. Lyu and Y. Zhao, Aptamer-decorated porous microneedles arrays for extraction and detection of skin interstitial fluid biomarkers, *Biosens. Bioelectron.*, 2021, **190**, 113404.
53 K. Takeuchi, N. Takama, B. Kim, K. Sharma, O. Paul and P. Ruther, Microfluidic chip to interface porous microneedles for ISF collection, *Biomed. Microdevices*, 2019, **21**, 28.
54 S. V. Puttaswamy, G. V. Lubarsky, C. Kelsey, X. Zhang, D. Finlay, J. A. McLaughlin and N. Bhalla, Nanophotonic-carbohydrate lab-on-a-microneedle for rapid detection of human cystatin C in finger-prick blood, *ACS Nano*, 2020, **14**, 11939–11949.
55 P. Liu, H. Du, Z. Wu, H. Wang, J. Tao, L. Zhang and J. Zhu, Hydrophilic and anti-adhesive modification of porous polymer microneedles for rapid dermal interstitial fluid extraction, *J. Mater. Chem. B*, 2021, **9**, 5476–5483.
56 Z. Gan, X. Qin, H. Liu, J. Liu and J. Qin, Recent advances in defined hydrogels in organoid research, *Bioact. Mater.*, 2023, **28**, 386–401.
57 M. C. Koetting, J. T. Peters, S. D. Steichen and N. A. Peppas, Stimulus-responsive hydrogels: Theory, modern advances, and applications, *Mater. Sci. Eng., R*, 2015, **93**, 1–49.
58 H. R. Culver, J. R. Clegg and N. A. Peppas, Analyte-responsive hydrogels: Intelligent materials for biosensing and drug delivery, *Acc. Chem. Res.*, 2017, **50**, 170–178.
59 A. V. Romanyuk, V. N. Zvezdin, P. Samant, M. I. Grenader, M. Zemlyanova and M. R. Prausnitz, Collection of analytes from microneedle patches, *Anal. Chem.*, 2014, **86**, 10520–10523.
60 E. Caffarel-Salvador, A. J. Brady, E. Eltayib, T. Meng, A. Alonso-Vicente, P. Gonzalez-Vazquez, B. M. Torrisi, E. M. Vicente-Perez, K. Mooney, D. S. Jones, S. E. Bell, C. P. McCoy, H. O. McCarthy, J. C. McElnay and R. F. Donnelly, Hydrogel-forming microneedle arrays allow detection of drugs and glucose in vivo: Potential for use in diagnosis and therapeutic drug monitoring, *PLoS One*, 2015, **10**, 145644.
61 R. Y. He, Y. Niu, Z. D. Li, A. Y. Li, H. Yang, F. Xu and F. Li, A hydrogel microneedle patch for point-of-care testing based on skin interstitial fluid, *Adv. Healthcare Mater.*, 2020, **9**, 1901201.
62 N. Xu, M. Zhang, W. Xu, G. Ling, J. Yu and P. Zhang, Swellable PVA/PVP hydrogel microneedle patches for the extraction of interstitial skin fluid toward minimally invasive monitoring of blood glucose level, *Analyst*, 2022, **147**, 1478–1491.
63 D. Al Sulaiman, J. Y. H. Chang, N. R. Bennett, H. Topouzi, C. A. Higgins, D. J. Irvine and S. Ladame, Hydrogel-coated microneedle arrays for minimally invasive sampling and sensing of specific circulating nucleic acids from skin interstitial fluid, *ACS Nano*, 2019, **13**, 9620–9628.
64 E. Laszlo, G. De Crescenzo, A. Nieto-Argüello, X. Banquy and D. Brambilla, Superswelling microneedle arrays for dermal interstitial fluid (prote)omics, *Adv. Funct. Mater.*, 2021, **31**, 2106061.
65 J. Zhu, X. Zhou, H. J. Kim, M. Qu, X. Jiang, K. Lee, L. Ren, Q. Wu, C. Wang, X. Zhu, P. Tebon, S. Zhang, J. Lee, N. Ashammakhi, S. Ahadian, M. R. Dokmeci, Z. Gu, W. Sun and A. Khademhosseini, Gelatin methacryloyl microneedle patches for minimally invasive extraction of skin interstitial fluid, *Small*, 2020, **16**, 1905910.
66 H. Chang, M. Zheng, X. Yu, A. Than, R. Z. Seeni, R. Kang, J. Tian, D. P. Khanh, L. Liu, P. Chen and C. Xu, A swellable microneedle patch to rapidly extract skin interstitial fluid for timely metabolic analysis, *Adv. Mater.*, 2017, **29**, 1702243.

67 D. F. S. Fonseca, P. C. Costa, I. F. Almeida, P. Dias-Pereira, I. Correia-Sa, V. Bastos, H. Oliveira, C. Vilela, A. J. D. Silvestre and C. S. R. Freire, Swellable gelatin methacryloyl microneedles for extraction of interstitial skin fluid toward minimally invasive monitoring of urea, *Macromol. Biosci.*, 2020, **20**, 2000195.

68 M. Wu, Y. Zhang, Q. Liu, H. Huang, X. Wang, Z. Shi, Y. Li, S. Liu, L. Xue and Y. Lei, A smart hydrogel system for visual detection of glucose, *Biosens. Bioelectron.*, 2019, **142**, 111547.

69 Y. Wang, H. Liu, X. Yang, Z. Shi, J. Li, L. Xue, S. Liu and Y. Lei, A responsive hydrogel-based microneedle system for minimally invasive glucose monitoring, *Smart Mater. Med.*, 2023, **4**, 69–77.

70 Y. N. Kalia, A. Naik, J. Garrison and R. H. Guy, Iontophoretic drug delivery, *Adv. Drug Delivery Rev.*, 2004, **56**, 619–658.

71 J. Yang, Y. Li, R. Ye, Y. Zheng, X. Li, Y. Chen, X. Xie and L. Jiang, Smartphone-powered iontophoresis-microneedle array patch for controlled transdermal delivery, *Microsyst. Nanoeng.*, 2020, **6**, 112.

72 T. Chang, H. Li, N. Zhang, X. Jiang, X. Yu, Q. Yang, Z. Jin, H. Meng and L. Chang, Highly integrated watch for noninvasive continual glucose monitoring, *Microsyst. Nanoeng.*, 2022, **8**, 25.

73 M. J. Tierney, J. A. Tamada, R. O. Potts, L. Jovanovic and S. Garg, Clinical evaluation of the GlucoWatch® biographer: a continual, non-invasive glucose monitor for patients with diabetes, *Biosens. Bioelectron.*, 2001, **16**, 621–629.

74 S. Kusama, K. Sato, Y. Matsui, N. Kimura, H. Abe, S. Yoshida and M. Nishizawa, Transdermal electroosmotic flow generated by a porous microneedle array patch, *Nat. Commun.*, 2021, **12**, 658.

75 X. Li, X. Huang, J. Mo, H. Wang, Q. Huang, C. Yang, T. Zhang, H.-J. Chen, T. Hang, F. Liu, L. Jiang, Q. Wu, H. Li, N. Hu and X. Xie, A fully integrated closed-loop system based on mesoporous microneedles-iontophoresis for diabetes treatment, *Adv. Sci.*, 2021, **8**, 2100827.

76 Z. Guo, H. Liu, W. Dai and Y. Lei, Responsive principles and applications of smart materials in biosensing, *Smart Mater. Med.*, 2020, **1**, 54–65.

77 C. Krafft, B. Dietzek and J. Popp, Raman and CARS microspectroscopy of cells and tissues, *Analyst*, 2009, **134**, 1046–1057.

78 N. C. Lindquist, C. D. L. de Albuquerque, R. G. Sobral-Filho, I. Paci and A. G. Brolo, High-speed imaging of surface-enhanced Raman scattering fluctuations from individual nanoparticles, *Nat. Nanotechnol.*, 2019, **14**, 981–987.

79 V. T. N. Linh, S.-G. Yim, C. Mun, J.-Y. Yang, S. Lee, Y. W. Yoo, D. K. Sung, Y.-I. Lee, D.-H. Kim, S.-G. Park, S. Y. Yang and H. S. Jung, Bioinspired plasmonic nanoflower-decorated microneedle for label-free intradermal sensing, *Appl. Surf. Sci.*, 2021, **551**, 149411.

80 C. Yuen and Q. Liu, Towards in vivo intradermal surface enhanced Raman scattering (SERS) measurements: silver coated microneedle based SERS probe, *J. Biophotonics*, 2014, **7**, 683–689.

81 C. Yuen and Q. Liu, Hollow agarose microneedle with silver coating for intradermal surface-enhanced Raman measurements: a skin-mimicking phantom study, *J. Biomed. Opt.*, 2015, **20**, 61102.

82 C. Kolluru, R. Gupta, Q. Jiang, M. Williams, H. G. Derami, S. Cao, R. K. Noel, S. Singamaneni and M. R. Prausnitz, Plasmonic paper microneedle patch for on-patch detection of molecules in dermal interstitial fluid, *ACS Sens.*, 2019, **4**, 1569–1576.

83 J. Ju, C. M. Hsieh, Y. Tian, J. Kang, R. Chia, H. Chang, Y. Bai, C. Xu, X. Wang and Q. Liu, Surface enhanced Raman spectroscopy based biosensor with a microneedle array for minimally invasive in vivo glucose measurements, *ACS Sens.*, 2020, **5**, 1777–1785.

84 J. E. Park, N. Yonet-Tanyeri, E. Vander Ende, A.-I. Henry, B. E. Perez White, M. Mrksich and R. P. Van Duyne, Plasmonic microneedle arrays for in situ sensing with surface-enhanced raman spectroscopy (SERS), *Nano Lett.*, 2019, **19**, 6862–6868.

85 C. Pan, X. Li, J. Sun, Z. Li, L. Zhang, W. Qian, P. Wang and J. Dong, A multiplexed sers-active microneedle for simultaneous redox potential and ph measurements in rat joints, *ACS Appl. Bio Mater.*, 2019, **2**, 2102–2108.

86 Y. Wang, H. Ni, H. Li, J. Chen, D. Zhang and L. Fu, Plasmonic microneedle arrays for rapid extraction, SERS detection, and inactivation of bacteria, *Chem. Eng. J.*, 2022, **442**, 136140.

87 C. D. Walkey and W. C. W. Chan, Understanding and controlling the interaction of nanomaterials with proteins in a physiological environment, *Chem. Soc. Rev.*, 2012, **41**, 2780–2799.

88 Y. C. Hsieh, C. Y. Lin, H. Y. Lin, C. T. Kuo, S. Y. Yin, Y. H. Hsu, H. F. Yeh, J. Wang and D. Wan, Controllable-swelling microneedle–assisted ultrasensitive paper sensing platforms for personal health monitoring, *Adv. Healthcare Mater.*, 2023, **13**, 2300321.

89 D. Nicholas, K. A. Logan, Y. Sheng, J. Gao, S. Farrell, D. Dixon, B. Callan, A. P. McHale and J. F. Callan, Rapid paper based colorimetric detection of glucose using a hollow microneedle device, *Int. J. Pharm.*, 2018, **547**, 244–249.

90 Y. Zeng, J. Wang, Z. Wang, G. Chen, J. Yu, S. Li, Q. Li, H. Li, D. Wen, Z. Gu and Z. Gu, Colloidal crystal microneedle patch for glucose monitoring, *Nano Today*, 2020, **35**, 100984.

91 R. He, H. Liu, T. Fang, Y. Niu, H. Zhang, F. Han, B. Gao, F. Li and F. Xu, A colorimetric dermal tattoo biosensor fabricated by microneedle patch for multiplexed detection of health-related biomarkers, *Adv. Sci.*, 2021, **8**, 2103030.

92 D. D. Zhu, L. W. Zheng, P. K. Duong, R. H. Cheah, X. Y. Liu, J. R. Wong, W. J. Wang, S. T. Tien Guan, X. T. Zheng and P. Chen, Colorimetric microneedle

patches for multiplexed transdermal detection of metabolites, *Biosens. Bioelectron.*, 2022, **212**, 114412.
93 H. Lee, G. Bonfante, Y. Sasaki, N. Takama, T. Minami and B. Kim, Porous microneedles on a paper for screening test of prediabetes, *Med. Devices Sens.*, 2020, **3**, 10109.
94 Z. Wang, H. Li, J. Wang, Z. Chen, G. Chen, D. Wen, A. Chan and Z. Gu, Transdermal colorimetric patch for hyperglycemia sensing in diabetic mice, *Biomaterials*, 2020, **237**, 119782.
95 W.-L. Hsu, C.-Y. Huang, Y.-P. Hsu, T.-L. Hwang, S.-H. Chang, H.-Y. J. Wang, L.-Y. Feng, S.-J. Tzou, K.-C. Wei and H.-W. Yang, On-skin glucose-biosensing and on-demand insulin-zinc hexamers delivery using microneedles for syringe-free diabetes management, *Chem. Eng. J.*, 2020, **398**, 125536.
96 J. Wang, P. W. H. Pinkse, L. I. Segerink and J. C. T. Eijkel, Bottom-up assembled photonic crystals for structure-enabled label-free sensing, *ACS Nano*, 2021, **15**, 9299–9327.
97 H. Liu, Y. Wang, Z. Shi, D. Tan, X. Yang, L. Xiong, G. Li, Y. Lei and L. Xue, Fast self-assembly of photonic crystal hydrogel for wearable strain and temperature sensor, *Small Methods*, 2022, **6**, 2200461.
98 A. K. Yetisen, N. Jiang, A. Fallahi, Y. Montelongo, G. U. Ruiz Esparza, A. Tamayol, Y. S. Zhang, I. Mahmood, S. A. Yang, K. S. Kim, H. Butt, A. Khademhosseini and S. H. Yun, Glucose-sensitive hydrogel optical fibers functionalized with phenylboronic acid, *Adv. Mater.*, 2017, **29**, 1606380.
99 C. Zhang, G. G. Cano and P. V. Braun, Linear and fast hydrogel glucose sensor materials enabled by volume resetting agents, *Adv. Mater.*, 2014, **26**, 5678–5683.
100 M. Elsherif, M. U. Hassan, A. K. Yetisen and H. Butt, Wearable contact lens biosensors for continuous glucose monitoring using smartphones, *ACS Nano*, 2018, **12**, 5452–5462.
101 M. Lu, X. Zhang, D. Xu, N. Li and Y. Zhao, Encoded structural color microneedle patches for multiple screening of wound small molecules, *Adv. Mater.*, 2023, **35**, 2211330.
102 X. Feng, J. Xu, Y. Liu and W. Zhao, Visual sensors of an inverse opal hydrogel for the colorimetric detection of glucose, *J. Mater. Chem. B*, 2019, **7**, 3576–3581.
103 J. Cai, W. Luo, J. Pan, G. Li, Y. Pu, L. Si, G. Shi, Y. Shao, H. Ma and J. Guan, Glucose-sensing photonic nanochain probes with color change in seconds, *Adv. Sci.*, 2022, **9**, 2105239.
104 H. Zheng, A. GhavamiNejad, P. GhavamiNejad, M. Samarikhalaj, A. Giacca and M. Poudineh, Hydrogel microneedle-assisted assay integrating aptamer probes and fluorescence detection for reagentless biomarker quantification, *ACS Sens.*, 2022, **7**, 2387–2399.
105 T. Saxl, F. Khan, D. R. Matthews, Z. L. Zhi, O. Rolinski, S. Ameer-Beg and J. Pickup, Fluorescence lifetime spectroscopy and imaging of nano-engineered glucose sensor microcapsules based on glucose/galactose-binding protein, *Biosens. Bioelectron.*, 2009, **24**, 3229–3234.
106 C. Tiangco, D. Fon, N. Sardesai, Y. Kostov, F. Sevilla, G. Rao and L. Tolosa, Fiber optic biosensor for transdermal glucose based on the glucose binding protein, *Sens. Actuators, B*, 2017, **242**, 569–576.
107 S. Brown, P. N. Zambrana, X. Ge, D. Bagdure, A. L. Stinchcomb, G. Rao and L. Tolosa, Minimally invasive technique for measuring transdermal glucose with a fluorescent biosensor, *Anal. Bioanal. Chem.*, 2018, **410**, 7249–7260.
108 J. Zhang, Y. Zheng, J. Lee, A. Hoover, S. A. King, L. Chen, J. Zhao, Q. Lin, C. Yu, L. Zhu and X. Wu, Continuous glucose monitoring enabled by fluorescent nanodiamond boronic hydrogel, *Adv. Sci.*, 2023, **10**, 2203943.
109 M. Sang, M. Cho, S. Lim, I. S. Min, Y. Han, C. Lee, J. Shin, K. Yoon, W.-H. Yeo, T. Lee, S. M. Won, Y. Jung, Y. J. Heo and K. J. Yu, Fluorescent-based biodegradable microneedle sensor array for tether-free continuous glucose monitoring with smartphone application, *Sci. Adv.*, 2023, **9**, 1765.
110 L. Wang, S. Xie, Z. Wang, F. Liu, Y. Yang, C. Tang, X. Wu, P. Liu, Y. Li, H. Saiyin, S. Zheng, X. Sun, F. Xu, H. Yu and H. Peng, Functionalized helical fibre bundles of carbon nanotubes as electrochemical sensors for long-term in vivo monitoring of multiple disease biomarkers, *Nat. Biomed. Eng.*, 2020, **4**, 159–171.
111 H. Lee, Y. J. Hong, S. Baik, T. Hyeon and D. H. Kim, Enzyme-based glucose sensor: From invasive to wearable device, *Adv. Healthcare Mater.*, 2018, **7**, 1701150.
112 K. Tian, M. Prestgard and A. Tiwari, A review of recent advances in nonenzymatic glucose sensors, *Mater. Sci. Eng., C*, 2014, **41**, 100–118.
113 M. Adeel, M. M. Rahman, I. Caligiuri, V. Canzonieri, F. Rizzolio and S. Daniele, Recent advances of electrochemical and optical enzyme-free glucose sensors operating at physiological conditions, *Biosens. Bioelectron.*, 2020, **165**, 112331.
114 S. P. Nichols, A. Koh, W. L. Storm, J. H. Shin and M. H. Schoenfisch, Biocompatible materials for continuous glucose monitoring devices, *Chem. Rev.*, 2013, **113**, 2528–2549.
115 A. A. Karyakin, O. V. Gitelmacher and E. E. Karyakina, Prussian blue-based first-generation biosensor. A sensitive amperometric electrode for glucose, *Anal. Chem.*, 2002, **67**, 2419–2423.
116 A. K. M. Kafi, S. Alim, R. Jose and M. M. Yusoff, Fabrication of a glucose oxidase/multiporous tin-oxide nanofiber film on Prussian blue–modified gold electrode for biosensing, *J. Electroanal. Chem.*, 2019, **852**, 113550.
117 R. Alhans, A. Singh, C. Singhal, J. Narang, S. Wadhwa and A. Mathur, Comparative analysis of single-walled and multi-walled carbon nanotubes for electrochemical sensing of glucose on gold printed circuit boards, *Mater. Sci. Eng., C*, 2018, **90**, 273–279.
118 H. Tang, F. Yan, P. Lin, J. Xu and H. L. W. Chan, Highly sensitive glucose biosensors based on organic electrochemical transistors using platinum gate electrodes modi-

fied with enzyme and nanomaterials, *Adv. Funct. Mater.*, 2011, **21**, 2264–2272.

119 J. Wang, J.-W. Mo, S. Li and J. Porter, Comparison of oxygen-rich and mediator-based glucose-oxidase carbon-paste electrodes, *Anal. Chim. Acta*, 2001, **441**, 183–189.

120 W. Schuhmann, T. J. Ohara, H. L. Schmidt and A. Heller, Electron transfer between glucose oxidase and electrodes via redox mediators bound with flexible chains to the enzyme surface, *J. Am. Chem. Soc.*, 2002, **113**, 1394–1397.

121 A. N. Sekretaryova, D. V. Vokhmyanina, T. O. Chulanova, E. E. Karyakina and A. A. Karyakin, Reagentless biosensor based on glucose oxidase wired by the mediator freely diffusing in enzyme containing membrane, *Anal. Chem.*, 2012, **84**, 1220–1223.

122 M. Marquitan, T. Bobrowski, A. Ernst, P. Wilde, J. Clausmeyer, A. Ruff and W. Schuhmann, Miniaturized amperometric glucose sensors based on polymer/enzyme modified carbon electrodes in the sub-micrometer scale, *J. Electrochem. Soc.*, 2018, **165**, G3008.

123 T. Bobrowski and W. Schuhmann, Long-term implantable glucose biosensors, *Curr. Opin. Electrochem.*, 2018, **10**, 112–119.

124 P. Rafighi, M. Tavahodi and B. Haghighi, Fabrication of a third-generation glucose biosensor using graphene-poly-ethyleneimine-gold nanoparticles hybrid, *Sens. Actuators, B*, 2016, **232**, 454–461.

125 Y. Degani and A. Heller, Electrical communication between redox centers of glucose oxidase and electrodes via electrostatically and covalently bound redox polymers, *J. Am. Chem. Soc.*, 1989, **111**, 2357–2358.

126 M. V. Jose, S. Marx, H. Murata, R. R. Koepsel and A. J. Russell, Direct electron transfer in a mediator-free glucose oxidase-based carbon nanotube-coated biosensor, *Carbon*, 2012, **50**, 4010–4020.

127 M. Tasviri, H. A. Rafiee Pour, H. Ghourchian and M. R. Gholami, Amine functionalized TiO_2 coated on carbon nanotube as a nanomaterial for direct electrochemistry of glucose oxidase and glucose biosensing, *J. Mol. Catal. B: Enzym.*, 2011, **68**, 206–210.

128 G. Manasa, R. J. Mascarenhas, N. P. Shetti, S. J. Malode, A. Mishra, S. Basu and T. M. Aminabhavi, Skin patchable sensor surveillance for continuous glucose monitoring, *ACS Appl. Bio Mater.*, 2022, **5**, 945–970.

129 S. Sharma, Z. Huang, M. Rogers, M. Boutelle and A. E. G. Cass, Evaluation of a minimally invasive glucose biosensor for continuous tissue monitoring, *Anal. Bioanal. Chem.*, 2016, **408**, 8427–8435.

130 J. R. Windmiller, G. Valdés-Ramírez, N. Zhou, M. Zhou, P. R. Miller, C. Jin, S. M. Brozik, R. Polsky, E. Katz, R. Narayan and J. Wang, Bicomponent microneedle array biosensor for minimally-invasive glutamate monitoring, *Electroanalysis*, 2011, **23**, 2302–2309.

131 D. Chen, C. Wang, W. Chen, Y. Chen and J. X. J. Zhang, PVDF-Nafion nanomembranes coated microneedles for in vivo transcutaneous implantable glucose sensing, *Biosens. Bioelectron.*, 2015, **74**, 1047–1052.

132 B. L. Zhang, Y. Yang, Z. Q. Zhao and X. D. Guo, A gold nanoparticles deposited polymer microneedle enzymatic biosensor for glucose sensing, *Electrochim. Acta*, 2020, **358**, 136917.

133 J. Gao, W. Huang, Z. Chen, C. Yi and L. Jiang, Simultaneous detection of glucose, uric acid and cholesterol using flexible microneedle electrode array-based biosensor and multi-channel portable electrochemical analyzer, *Sens. Actuators, B*, 2019, **287**, 102–110.

134 Y. Liu, Q. Yu, X. Luo, L. Yang and Y. Cui, Continuous monitoring of diabetes with an integrated microneedle biosensing device through 3D printing, *Microsyst. Nanoeng.*, 2021, **7**, 75.

135 H. Teymourian, C. Moonla, F. Tehrani, E. Vargas, R. Aghavali, A. Barfidokht, T. Tangkuaram, P. P. Mercier, E. Dassau and J. Wang, Microneedle-based detection of ketone bodies along with glucose and lactate: Toward real-time continuous interstitial fluid monitoring of diabetic ketosis and ketoacidosis, *Anal. Chem.*, 2020, **92**, 2291–2300.

136 J. Trzebinski, S. Sharma, A. R. Moniz, K. Michelakis, Y. Zhang and A. E. G. Cass, Microfluidic device to investigate factors affecting performance in biosensors designed for transdermal applications, *Lab Chip*, 2012, **12**, 348–352.

137 G. Valdés-Ramírez, Y.-C. Li, J. Kim, W. Jia, A. J. Bandodkar, R. Nuñez-Flores, P. R. Miller, S.-Y. Wu, R. Narayan, J. R. Windmiller, R. Polsky and J. Wang, Microneedle-based self-powered glucose sensor, *Electrochem. Commun.*, 2014, **47**, 58–62.

138 A. Caliò, P. Dardano, V. Di Palma, M. F. Bevilacqua, A. Di Matteo, H. Iuele and L. De Stefano, Polymeric microneedles based enzymatic electrodes for electrochemical biosensing of glucose and lactic acid, *Sens. Actuators, B*, 2016, **236**, 343–349.

139 K. B. Kim, H. Choi, H. J. Jung, Y.-J. Oh, C.-H. Cho, J. H. Min, S. Yoon, J. Kim, S. J. Cho and H. J. Cha, Mussel-inspired enzyme immobilization and dual real-time compensation algorithms for durable and accurate continuous glucose monitoring, *Biosens. Bioelectron.*, 2019, **143**, 111622.

140 M. Dervisevic, M. Alba, L. Yan, M. Senel, T. R. Gengenbach, B. Prieto-Simon and N. H. Voelcker, Transdermal electrochemical monitoring of glucose via high-density silicon microneedle array patch, *Adv. Funct. Mater.*, 2022, **32**, 2009850.

141 P. Bollella, S. Sharma, A. E. G. Cass, F. Tasca and R. Antiochia, Minimally invasive glucose monitoring using a highly porous gold microneedles-based biosensor: characterization and application in artificial interstitial fluid, *Catalysts*, 2019, **9**, 580.

142 P. Bollella, S. Sharma, A. E. G. Cass and R. Antiochia, Minimally-invasive microneedle-based biosensor array for simultaneous lactate and glucose monitoring in artificial interstitial fluid, *Electroanalysis*, 2019, **31**, 374–382.

143 K. B. Kim, W.-C. Lee, C.-H. Cho, D.-S. Park, S. J. Cho and Y.-B. Shim, Continuous glucose monitoring using a microneedle array sensor coupled with a wireless signal transmitter, *Sens. Actuators, B*, 2019, **281**, 14–21.

144 M. A. Invernale, B. C. Tang, R. L. York, L. Le, D. Y. Hou and D. G. Anderson, Microneedle electrodes toward an amperometric glucose-sensing smart patch, *Adv. Healthcare Mater.*, 2014, **3**, 338–342.

145 H.-J. Kil, S.-R. Kim and J.-W. Park, A self-charging supercapacitor for a patch-type glucose sensor, *ACS Appl. Mater. Interfaces*, 2022, **14**, 3838–3848.

146 S. Park, H. Boo and T. D. Chung, Electrochemical non-enzymatic glucose sensors, *Anal. Chim. Acta*, 2006, **556**, 46–57.

147 M. Wei, Y. Qiao, H. Zhao, J. Liang, T. Li, Y. Luo, S. Lu, X. Shi, W. Lu and X. Sun, Electrochemical non-enzymatic glucose sensors: recent progress and perspectives, *Chem. Commun.*, 2020, **56**, 14553–14569.

148 Q. Dong, H. Ryu and Y. Lei, Metal oxide based non-enzymatic electrochemical sensors for glucose detection, *Electrochim. Acta*, 2021, **370**, 137744.

149 T. Rasheed and K. Rizwan, Metal-organic frameworks based hybrid nanocomposites as state-of–the-art analytical tools for electrochemical sensing applications, *Biosens. Bioelectron.*, 2022, **199**, 113867.

150 H. Yang, Z. Wang, Q. Zhou, C. Xu and J. Hou, Nanoporous platinum-copper flowers for non-enzymatic sensitive detection of hydrogen peroxide and glucose at near-neutral pH values, *Microchim. Acta*, 2019, **186**, 631.

151 W. C. Lee, K. B. Kim, N. G. Gurudatt, K. K. Hussain, C. S. Choi, D. S. Park and Y. B. Shim, Comparison of enzymatic and non-enzymatic glucose sensors based on hierarchical Au-Ni alloy with conductive polymer, *Biosens. Bioelectron.*, 2019, **130**, 48–54.

152 A. Yu, S. Moon, T. Kwon, Y. B. Cho, M. H. Kim, C. Lee and Y. Lee, Au-Ir alloy nanofibers synthesized from Au-Ir/IrO2 composites via thermal hydrogen treatment: Application for glucose oxidation, *Sens. Actuators, B*, 2020, **310**, 127822.

153 T. Zhe, X. Sun, Y. Liu, Q. Wang, F. Li, T. Bu, P. Jia, Q. Lu, J. Wang and L. Wang, An integrated anode based on porous Ni/Cu(OH)2 nanospheres for non-enzymatic glucose sensing, *Microchem. J.*, 2019, **151**, 104197.

154 S. Bilal, W. Ullah and A. U. H. A. Shah, Polyaniline@CuNi nanocomposite: A highly selective, stable and efficient electrode material for binder free non-enzymatic glucose sensor, *Electrochim. Acta*, 2018, **284**, 382–391.

155 M. Wang, D. He, M. Huang, X. Wang and P. Jiang, In situ growth of Ni-B nanoparticles on Ni foam: An efficient 3D integrated anode for enzyme-free glucose detection, *J. Alloys Compd.*, 2019, **786**, 530–536.

156 Q. Wa, W. Xiong, R. Zhao, Z. He, Y. Chen and X. Wang, Nanoscale $Ni(OH)_x$ films on carbon cloth prepared by atomic layer deposition and electrochemical activation for glucose sensing, *ACS Appl. Nano Mater.*, 2019, **2**, 4427–4434.

157 Y. Zhang, L. Su, D. Manuzzi, H. V. E. de los Monteros, W. Jia, D. Huo, C. Hou and Y. Lei, Ultrasensitive and selective non-enzymatic glucose detection using copper nanowires, *Biosens. Bioelectron.*, 2012, **31**, 426–432.

158 W. Na, J. Lee, J. Jun, W. Kim, Y. K. Kim and J. Jang, Highly sensitive copper nanowire conductive electrode for nonenzymatic glucose detection, *J. Ind. Eng. Chem.*, 2019, **69**, 358–363.

159 Q. Wang, Y. Chen, R. Zhu, M. Luo, Z. Zou, H. Yu, X. Jiang and X. Xiong, One-step synthesis of Co(OH)F nanoflower based on micro-plasma: As an effective non-enzymatic glucose sensor, *Sens. Actuators, B*, 2020, **304**, 127282.

160 W. Raza and K. Ahmad, A highly selective Fe@ZnO modified disposable screen printed electrode based non-enzymatic glucose sensor (SPE/Fe@ZnO), *Mater. Lett.*, 2018, **212**, 231–234.

161 J. Gao, T. Meng, S. Lu, X. Ma, Y. Zhang, D. Fu, Z. Lu and C. M. Li, Manganese-doped tremella-like nickel oxide as biomimetic sensors toward highly sensitive detection of glucose in human serum, *J. Electroanal. Chem.*, 2020, **863**, 114071.

162 X. Tang, B. Zhang, C. Xiao, H. Zhou, X. Wang and D. He, Carbon nanotube template synthesis of hierarchical $NiCoO_2$ composite for non-enzyme glucose detection, *Sens. Actuators, B*, 2016, **222**, 232–239.

163 S. K. Krishnan, E. Singh, P. Singh, M. Meyyappan and H. S. Nalwa, A review on graphene-based nanocomposites for electrochemical and fluorescent biosensors, *RSC Adv.*, 2019, **9**, 8778–8881.

164 Y. Yoon, G. S. Lee, K. Yoo and J. B. Lee, Fabrication of a microneedle/CNT hierarchical micro/nano surface electrochemical sensor and its in-vitro glucose sensing characterization, *Sensors*, 2013, **13**, 16672–16681.

165 S. J. Lee, H. S. Yoon, X. Xuan, J. Y. Park, S.-J. Paik and M. G. Allen, A patch type non-enzymatic biosensor based on 3D SUS micro-needle electrode array for minimally invasive continuous glucose monitoring, *Sens. Actuators, B*, 2016, **222**, 1144–1151.

166 S. R. Chinnadayyala, I. Park and S. Cho, Nonenzymatic determination of glucose at near neutral pH values based on the use of nafion and platinum black coated microneedle electrode array, *Microchim. Acta*, 2018, **185**, 250.

167 S. R. Chinnadayyala, J. Park, A. T. Satti, D. Kim and S. Cho, Minimally invasive and continuous glucose monitoring sensor based on non-enzymatic porous platinum black-coated gold microneedles, *Electrochim. Acta*, 2021, **369**, 137691.

168 A. Jina, M. J. Tierney, J. A. Tamada, S. McGill, S. Desai, B. Chua, A. Chang and M. Christiansen, Design, development, and evaluation of a novel microneedle array-based continuous glucose monitor, *J. Diabetes Sci. Technol.*, 2014, **8**, 483–487.

169 J. Yang, S. Zheng, D. Ma, T. Zhang, X. Huang, S. Huang, H.-J. Chen, J. Wang, L. Jiang and X. Xie, Masticatory system–inspired microneedle theranostic platform for intelligent and precise diabetic management, *Sci. Adv.*, 2022, **8**, 6900.

170 L. Zheng, D. Zhu, W. Wang, J. Liu, S. T. G. Thng and P. Chen, A silk-microneedle patch to detect glucose in the interstitial fluid of skin or plant tissue, *Sens. Actuators, B*, 2022, **372**, 132626.